Resource Allocation in Full-Duplex Multi-User RIS-Assisted Wireless-Powered IIoT Networks

Reynah Akwafo, Samuel Kwamena Menanor, Derek Kwaku Pobi Asiedu, Samir Saoudi, Ji-Hoon Yun, Kyoung-Jae Lee

Resource Allocation in Full-Duplex Multi-User RIS-Assisted Wireless-Powered IIoT Networks

Reynah Akwafo, Samuel Kwamena Menanor, Derek Kwaku Pobi Asiedu, *Member, IEEE*, Samir Saoudi, *Senior Member, IEEE*, Ji-Hoon Yun, *Senior Member, IEEE*, and Kyoung-Jae Lee, *Senior Member, IEEE*

***Abstract*—This paper examines radio resource allocation in a full-duplex (FD) reconfigurable intelligent surface (RIS)-assisted wireless-powered (WP) industrial internet-of-Things (IIoT) communication network. The system model includes an FD access point (FD-AP) that communicates with FD energy harvesting (EH) multi-users (MUs), referred to as an FD-FD RIS-assisted WP-IIoT network. The FD-AP is equipped with two sets of multiple antennas: one set for downlink (DL) energy beamforming and another for uplink (UL) information signal reception. The FD-MUs have one antenna for DL energy signal reception and another for UL information transmission. This paper addresses the UL sum-rate maximization problem for the FD-FD RIS-assisted WP-IIoT system by jointly optimizing the RIS phase shift and power resources. Additionally, this paper presents two benchmarks as specific cases of the FD-FD RIS-assisted WP-IIoT system model, namely, (i) FD-HD RIS-assisted WP-IIoT network: FD AP and half-duplex (HD) two MUs groups, and (ii) HD-HD RIS-assisted WP-IIoT network: HD AP and HD MUs. The numerical results demonstrate that the FD-FD system outperforms both benchmarks in the low transmit power regime. Also, compared to the baseline non-RIS-assisted WP-IIoT network, the RIS-assisted WP-IIoT network achieved a significant UL sum-rate gain.**

***Index Terms*—Full duplex (FD), reconfigurable intelligent surface (RIS), energy harvesting (EH), sum-rate, resource allocation.**

I. Introduction

AS Internet-of-Things (IoT) networks are rapidly deployed in manufacturing settings, this has given rise to the concept of industrial IoT (IIoT) networks [2]. IIoT networks are transforming traditional industrial automation and process control by facilitating seamless connectivity among components such as sensors and industrial equipment across various locations and enabling real-time automation and decision-making [3]–[5]. While IIoT networks offer enhanced capabilities and benefits, including increased efficiency and productivity [5], [6], their widespread deployment, compactness and mobility of wireless devices encounter significant challenges. One significant challenge is the energy constraints on the battery-operated devices, which necessitate periodic battery replacements or frequent recharges, as well as maintaining reliable communication in the harsh industrial wireless communication environments [7]–[9]. This issue raises maintenance costs and contradicts the need for green communications and a self-sustainable IIoT network because of climate change concerns.

The energy constraint issue faced by IIoT devices has been notably addressed by recent advancements in energy harvesting (EH) technologies, such as wireless powered communication networks (WPCN) [7], [8], [10], [11]. These technologies enable self-sustaining devices to harvest energy from near and far-field radio frequency (RF) sources. In particular, WPCN integrates wireless energy transfer (WET) and wireless information transfer (WIT), where a hybrid access point (AP) transmits energy signals to the IIoT devices during downlink (DL) communication. The energy signals received in the DL are stored and later utilized to transmit information signals from the IIoT devices to the AP in the uplink (UL) [7], [8], [10]. Although WPCN is a promising technology that ensures a stable power source for IIoT devices, it still encounters significant network challenges in practical deployment due to severe signal loss caused by RF signal attenuation over long distances [7], [12]. Therefore, more effective and cost-efficient solutions are needed to enhance the DL WET. Advanced techniques, such as relaying and massive multiple-input-multiple-output (massive MIMO), can improve spectral efficiency (SE) [13]. However, these techniques often lead to increased network energy consumption and hardware costs [12], [14]. Conversely, to facilitate and expand EH and information transfer coverage areas, reconfigurable intelligent surfaces (RIS), composed of numerous passive, energy-efficient, and low-cost reflecting elements, can be deployed within IIoT networks to enhance coverage and spatial diversity [15], [16].

An RIS can modify and dynamically adjust the reflecting elements to control the reflected RF signals that are incident upon it [17]. Therefore, integrating RIS with WPCN technologies serves as an effective solution for achieving efficient and extended coverage of a self-sustaining IIoT network using RF EH. However, RIS may suffer from EH inefficiencies due

This work was partially presented at IEEE VTC spring 2025 in [1] containing the system analysis results without optimization and consideration of threshold energy harvesting model.

Corresponding author: Kyoung-Jae Lee (kyoungjae@cau.ac.kr).

R. Akwafo, and S. K. Menanor are with the Department of Electronic Engineering, Hanbat National University, Daejeon 34158, South Korea. (Emails: reynah.akwafo@edu.hanbat.ac.kr, and smenanor@edu.hanbat.ac.kr)

S. K. Menanor is also affiliated with the Department of Electronic Engineering, Ho Technical University, Ho, Ghana. (Email: smenanor@edu.hanbat.ac.kr)

D. K. P. Asiedu, and S. Saoudi are affiliated with the Lab-STICC Laboratory of the Department of Mathematical and Electrical Engineering, IMT Atlantique, Brest 29200, France. (Emails: kwakupobi@ieee.org, and samir.saoudi@imt-atlantique.fr)

Ji-Hoon Yun is with the Department of Information and Electrical Engineering, Seoul National University of Science and Technology, Seoul 01811, South Korea. (Email: jhyun@seoultech.ac.kr)

K.-J. Lee is with the School of Electrical and Electronics Engineering, Chung-Ang University, Seoul 06974, South Korea. (Email: kyoungjae@cau.ac.kr)

to issues such as double fading and the absence of a direct channel between the access point (AP) and IIoT devices, resulting in reduced SE. Consequently, establishing a direct link is essential to enhance the spectral efficiency. Compared to its half-duplex (HD) counterpart, full-duplex (FD) transmission can improve the SE of the RIS-assisted IIoT network [8]. Unlike HD systems that alternate between information and energy transfer over different dedicated time slots, FD systems allow DL WET and UL WIT to occur simultaneously using the same communication resources. This improves SE and reduces latency by eliminating the need for separate time slots [8]. Although FD transmission has the potential to increase SE, it requires complex self-interference cancellation (SIC) methods to effectively mitigate self interference (SI) [8], [18].

To reap the above benefits of integrating RIS into WPCN to provide signal coverage for devices in coverage-limited areas, this work proposes a unique WPCN IIoT system architecture in which both the DL and the UL transmission occur simultaneously via the direct channel and reflection of the RIS, thus potentially enhancing the spectral efficiency and the amount of energy harvested. The system consists of an FD AP equipped with a dual-set multi-antenna consisting of WET DL transmitter and WIT UL receiver antennas, and communicates with a dual-set (i.e., single-antenna DL WET receiver and single-antenna UL WIT transmitter) FD-MUs. For more insight, two special cases of the system model presented are considered. The first scenario considers an FD AP RIS-assisted WPCN system with HD MUs, while the second scenario discusses an HD AP RIS-assisted WPCN system with HD MUs, therefore, the operations of DL WET and UL WIT are orthogonal over time. In addition, the IIoT network resources are optimized to improve system performance.

The rest of this paper is organized as follows. Section II discusses the related works. Section III, describes the RIS-assisted WP-IIoT system model and problem formulation. Section IV contains the derived closed-form solutions and the alternating optimization (AO) algorithms. Section V contains the simulation results. Finally, section VI concludes the paper.

Notations: Capital letter bold ($\mathbf{A}$), small-letter bold ($\mathbf{a}$) and small-letter (a) alphabets denote a matrix, a vector and a scalar variable, respectively. $\mathbf{A} \in \mathbb{C}^{N\times M}$ is a matrix with dimensions N by M and $\mathbf{a} \in \mathbb{C}^{N}$ represents a vector with dimensions N by 1. h^* and h^H represent the conjugate transpose and transpose of variable h, respectively. $\mathcal{CN}(0,1)$ denotes circularly symmetric complex Gaussian random variable with zero mean and unit variance. A summary of frequently used variables and abbreviations are respectively outlined in Tables I and II.

TABLE I: Summary of Frequently Used Variables

Variable	Definition
K	Total Number of users communicating with the AP
K_1	Number of users communication with the AP in DL
K_2	Number of users communicating with the AP in UL
S_1	Number of users in DL group
S_2	Number of users in UL group
M	Total number of antennas
M_{t}	Number of AP transmit antenna
M_{r}	Number of receive antennas
N	Number of RIS elements
γ_k	Received SINR at MU k
τ_1	Time allocation for WET (Phase 1)
τ_2	Time allocation for WIT (Phase 2)
$\mathbf{h}_{\mathrm{e},k}$	Effective DL transmission channel
$\mathbf{f}_{\mathrm{e},k}$	Effective UL transmission channel
ϵ_{DL}	DL distance dependent pathloss
κ_{DL}	Rician K-factor between AP-RIS
$\kappa_{\mathrm{DL},k}$	Rician K-factor between RIS-MU
$\mathbf{h}_{\mathrm{D},k}$	DL channel from AP to MU k
$\mathbf{H}_{\mathrm{D,R}}$	DL channel from AP to RIS
$\mathbf{h}_{\mathrm{R},k}$	DL channel from RIS to MU k
$\mathbf{h}_{k,\mathrm{U}}$	UL channel from MU k to AP
$\mathbf{h}_{k,\mathrm{R}}$	UL channel from MU K to RIS
$\mathbf{H}_{\mathrm{R,U}}$	UL channel from RIS to AP k
$\mathbf{H}_{\mathrm{AP}}$	SI channel at the AP k
$\hat{\mathbf{G}}$	Effective SI channel at the AP k

TABLE II: Summary of Frequently Used Abbreviations

Abbreviation	Definition
AP	Access Point
CoI	Co-channel Interference
CSI	Channel State Information
DL	Downlink
EH	Energy Harvesting
FD	Full-Duplex
HD	Half-Duplex
IoT	Internet of Things
IIoT	Industrial Internet of Things
Imp-CSI	Imperfect Channel State Information
Imp-SIC	Imperfect Self Interference Cancellation
MIMO	Multiple-Input-Multiple-Output
PSR	Power Splitting Ratio
PS	Power Station
RF	Radio Frequency
RIS	Reconfigurable Intelligent Surface
SI	Self-Interference
TDD	Time Division Duplexing
TS	Time Switching
UP	Uplink
WET	Wireless Energy Transfer
WIT	Wireless Information Transfer
WMMSE	Weighted Minimum Mean Squared Error
WPCN	Wireless Powered Communication Network
WPT	Wireless Power Transfer

II. Related Works

Various works have investigated non-RIS-assisted WPCN system models in works such as [8], [19], [24]–[29]. However, this work focuses on RIS-assisted WPCN system models. Therefore, the literature reviewed below consists of novel works on RIS-assisted WPCN which are found in [1], [7], [10], [16], [17], [20], [22], [23].

A. Current State-of-The-Art: Exiting Works

For instance, the work studied in [8] has investigated WPCN protocols to facilitate communication between an FD AP and MUs. The FD AP has multiple antennas and operates in FD mode, while MUs are HD single antenna devices. Each MU communicating with the FD AP is assigned to one of two groups based on the time allocation and channel access for either UL or DL. To maximize the UL sum-rate, a weighted sum-rate maximization problem is formulated to

TABLE III: Summary of comparison with related works.

Reference	Objective	Technology					UE group
		RIS	EH Model	EH Recycling	BS	Users	
[7]	Sum-rate Maximization	✔	Power threshold	✘	HD-SISO	HD-MU	✘
[8]	Weighted sum-rate maximization	✘	Power threshold	✘	FD-MIMO	HD-MU	✔
[10]	Sum-rate optimization	✔	Sigmoid	✘	FD-MIMO	HD-MU	✘
[16]	Sum throughput maximization	✔	Power threshold	✘	HD-SISO	HD-MU	✔
[17]	Sum throughput maximization	✔	Sigmoid	✘	HD-SISO	HD-MU	✘
[19]	UL fair-throughput maximization	✘	Sigmoid	✘	FD-MIMO	HD-MU	✘
[20]	Rate and energy-efficiency maximization	✔	Sigmoid	✘	HD-SISO	HD-SU	✘
[21]	SI minimization and rate maximization	✔	✘	✘	FD-MIMO	HD-MU	✔
[22]	Weighted sum-throughput optimization	✔	Sigmoid	✘	FD-MIMO	HD-MU	✘
[23]	Weighted sum-throughput maximization	✔	Sigmoid	✘	FD-MIMO	FD-MU	✘
[1]	Sum-rate Analysis	✔	Power Threshold	✔	FD-MIMO	FD-MU	✘
This work	Sum-rate maximization	✔	Multi-stage rectifier	✔	FD-MIMO	FD-MU	✘

jointly optimize the channel assignment, time resource, and power resource allocations. Also, in [19], the authors studied multi-antenna resource scheduling for an FD-aided WPCN system, where HD single antenna MUs harvest energy from the FD-AP in the DL to power their own WIT. To support MUs, this FD-WPCN system adopts a classic TDMA protocol. The UL fair-throughput of MUs is maximized by joint design of the transceiver beamformer, resource allocation, and user scheduling. However, the study in [7] proposed a hybrid-relaying scheme designed to simultaneously enhance the performance of DL energy transfer from an AP and UL data transfer from users to the AP. Using a proposed time switching (TS) and power splitting ratio (PSR), the RIS can switch between EH and signal reflection in the TS scheme or adjust its reflection amplitude in the PSR scheme. The RIS and users are each equipped with an EH circuit. The HAP and users have a single antenna each, and the mode of transmission in this system is TDMA. By formulating sum-rate maximization problems for the TS and PS schemes, both the RIS phase shifts and network resource allocation were jointly optimized for EH and WIT by proposing a two-step algorithm to obtain a near-optimal solution with accuracy. In [16], the authors introduced an RIS-assisted wireless-powered heterogeneous network consisting of two heterogeneous groups of devices. Specifically, one group of devices is charged by external energy supplies (i.e., EH devices), while the other group of devices is powered by internal energy supplies (i.e., non-EH devices). The EH devices harvest energy signals from a separate power station (PS) via the RIS in the DL, and both groups perform information transfer through the RIS with an AP in the UL. The PS, AP, and devices have single antennas, and the devices communicate with the AP in TDMA mode. The RIS is deployed to enhance the DL WET and UL WIT. Therefore, a sum throughput maximization problem was formulated subject to the constraints of individual energy consumption, transmission time scheduling, and RIS phase shifts.

In [17], the authors examined a new transmission policy for resource allocation in an RIS-empowered IoT system. Similar to the system architecture in [16], an energy station wirelessly charges multiple IoT devices in the DL, and these devices transmit their data signals to the AP in the UL. A specific scenario is considered where circuit power consumption is overlooked. The RIS phase shift, transfer time scheduling, and PSR are optimized to maximize the sum throughput. The work in [20] explored single-user achievable rate maximization in an active RIS-assisted WPCN where both the HAP and the user have single antennas, and communication between HAP and UE is TDD. The active RIS phase shifts are optimized in both WPT and WIT phases, and the time allocation is optimized to maximize the achievable rate. The authors in [21] jointly optimized the precoder matrix and RIS phase shifts to enhance both UL and DL communication. The work in [10] investigated the performance of RIS enhanced FD WPCN where a HAP concurrently transmits energy and receives signal. A sum-rate maximization problem is formulated, and iterative algorithms are proposed to determine dynamic or static beamforming across uplink and downlink time slots. The authors in [22] studied an RIS-aided FD WPCN where a hybrid node (HN) operating in FD mode transmits information to MU devices in the DL, while receiving energy signals from a PS in the UL, with both processes supported by an RIS. The weighted sum throughput is examined by jointly optimizing the active transmit beamformer at the PS and HN, along with the passive RIS phase shifts.

Furthermore, the work in [23] investigated an RIS-aided MIMO FD WPCN system, where an FD-HN broadcasts energy signals to multiple devices for their EH in DL and receives information signals from the devices in the UL with the help of an RIS. Both nodes have multiple antennas, and using a designed time scheduling transmission protocol, a weighted sum-throughput maximization optimization problem is formulated by jointly optimizing the DL and UL time allocation, precoding matrices at devices, transmit covariance matrices at the FD-AP, and RIS phase shifts. Additionally, in [1], the authors investigated an FD RIS-assisted WPCN system where both the multi-antenna AP and EH MUs operate in FD mode. Energy recycling is considered at the MUs, and the RIS functions as a non-EH device. The sum-rate performance is analyzed with random RIS phase shifts.

B. Beyond State-of-The-Art: Contributions

Motivated by the above discussions, this paper examines a scenario involving all devices operating in an FD mode under imperfect SIC (imp-SIC) conditions in an RIS-assisted IIoT

network. The system comprises an FD-AP and FD-MU EH IoT-enabled sensor devices (FD-MUs) in an IIoT network. The overall objective of the system is to support simultaneous WET and WIT by exploiting the RIS to enhance both WET and WIT phases. The goal of this work is to maximize the system UL sum-rate by jointly designing the transceiver beamforming at the FD-AP and the transmit power at the FD-MU. In the considered FD RIS-assisted WP-IIoT system, the SI at the FD-AP arises due to its simultaneous transmit and receive operation. Similarly, the FD-MUs experience a loop-back SI, which impacts energy harvesting. Table III provides a brief comparison of this study with previous RIS-assisted WPCN works. The main contributions of this paper can be summarized as follows.

- ***System architecture:*** In this study, unlike existing works, a unique FD-FD RIS-assisted WP-IIoT system is proposed, in which the FD-AP simultaneously performs DL RF energy transfer and receives UL messages from FD-MUs. Given the significant power loss incurred as the distance between the FD-AP and FD-MUs increases, an RIS device is introduced into the network to enhance the performance of both DL WET and UL WIT phases concurrently. The uniqueness in this proposed system architecture lies in the consideration of all FD nodes in an RIS-assisted WPCN system scenario, which have not yet been considered. In addition, two special cases: FD-HD and HD-HD RIS-assisted WP-IIoT systems are presented and used as benchmarks. Importantly, these benchmark cases are examined within the same framework, which has not been considered in other works, but mostly studied separately in reviewed literature.
- ***Energy scavenging :*** To distinguish this work from other FD RIS-assisted WPCN research works, where MUs are typically restricted to time-division HD operation, such as in [10], [19], [22], [23], our system model considers the effective loop-back SI at the FD-MUs as recycled RF energy that contributes to the energy harvested, which is yet to be investigated. This novel method of recycling the effective loop-back SI at FD-MUs as an additional energy source is a distinct feature that has not been investigated in existing RIS-assisted WPCN studies. Moreover, the proposed system adopts the multi-stage rectifier circuit EH model similar to the EH model proposed in [30], which is more realistic than the linear, sigmoid, or threshold EH models leveraged in prior literature.
- ***System imperfections:***In addition to the perfect CSI scenario considered in [7], [8], [16], [17], [20]–[22], this work investigates the impact of imperfect channel state information (imp-CSI) at the FD-AP on the UL sum-rate and FD-MUs EH, thereby reflecting practical conditions where channel gains cannot be perfectly estimated. Given the complexity of channel estimation through the RIS, we adopt the approach in [8] for tractability. Furthermore, since the FD-AP experiences SI due its FD operation, imperfect SIC at the FD-AP is considered for the RIS-assisted WP-IIoT system model.
- ***System optimization and efficacy:*** Finally, two optimization problems are formulated to cover the proposed system and the benchmarks. The proposed FD-FD system model sum-rate is maximized by jointly optimizing the AP transmit and receive beamformers, transmit powers of the AP and MUs, and the RIS phase shift. For the FD-HD and HD-HD benchmark systems, MU resource and time allocation are also optimized. Based on the solutions, an AO algorithm is proposed for the FD-FD system and its benchmarks. Additionally, the computational complexity and overhead cost analysis for the various system configuration algorithm implementations are presented. The proposed FD-FD system is compared to the FD-HD and HD-HD system benchmarks in simulations, where the FD-FD is shown to be superior in certain instances compared to the benchmarks.

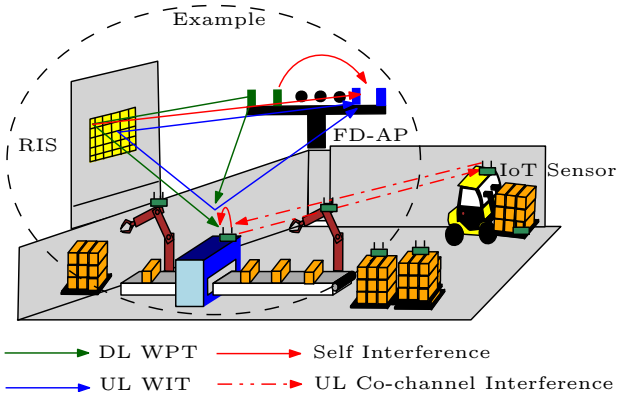

Fig. 1: FD-FD RIS-assisted WP-IIoT network system model.

III. The FD-FD RIS-Assisted WP-IIoT Network

In this section, the FD-FD RIS-assisted WP-IIoT system is presented. As shown in Fig. 1, the IIoT communication system consists of an FD-AP, an RIS, and K EH FD-MUs, where both the DL WET and UL WIT occur simultaneously over the same frequency. However, to enable efficient EH at the MUs due to the large attenuation over long distances, an RIS having N passive reflecting elements with adjustable phase shifts is introduced to extend the coverage area and increase spatial diversity of the WET signals. This implies that there is a direct link between the FD-AP and EH FD-MUs. The FD-AP is equipped with M_{t} DL WET antennas and M_{r} UL WIT receive antennas[1]. Also, each FD-MU is equipped with two antennas, one is a DL WET and the other is a UL WIT.

In this system model, it is assumed that the RIS is a non-EH device and only passively beamforms the DL WET and UL WIT signals[2]. Also, imp-CSI at the FD-AP, which leads to imp-SIC at the FD-AP, are assumed. The CSI of all links can be obtained using existing channel estimation approaches available in literature, such as [31]. The individual channel elements are modeled with estimation errors as

$$h_z = \hat{h}_z + \tilde{h}_z, \tag{1}$$

where, $\hat{h}_z \sim \mathcal{CN}(0, 1-\sigma_z^2)$ is the estimated channel and $\tilde{h}_z \sim \mathcal{CN}(0, \sigma_z^2)$ is the channel estimation error, where σ_z^2

[1]Note, in this paper, it is assumed $M_{\mathrm{t}} = M_{\mathrm{r}} = M$.
[2]For future work, EH RIS will be considered.

$$\mathrm{y}_k^{\mathrm{DL}} = \underbrace{(\mathbf{h}_{\mathrm{R},k}\boldsymbol{\Phi}\mathbf{H}_{\mathrm{D,R}} + \mathbf{h}_{\mathrm{D},k})\sum_{k=1}^{K}\mathbf{p}_k s_k^{\mathrm{DL}}}_{\text{Energy signal}} + \underbrace{\sum_{j\neq k}^{K}(\mathbf{h}_{\mathrm{R},k}\boldsymbol{\Phi}\mathbf{h}_{j,\mathrm{R}} + h_{j,k})\sqrt{P_j^{\mathrm{UL}}}s_j^{\mathrm{UL}}}_{\text{UL co-channel interference}} + \underbrace{\sqrt{P_k^{\mathrm{UL}}}(\mathbf{h}_{\mathrm{R},k}\boldsymbol{\Phi}\mathbf{h}_{k,\mathrm{R}} + h_k)s_k^{\mathrm{UL}}}_{\text{Energy Recycling at FD-MU } k} + \underbrace{\mathrm{n}_k^{\mathrm{DL}}}_{\text{Noise}} \tag{2}$$

$$\tilde{P}_k^{\mathrm{EH}} = \frac{\beta_k^2 R_{\mathrm{At},k}^2\left(\sum_{k=1}^{K}|\mathbf{h}_{\mathrm{e},k}\mathbf{p}_k|^2 + P_k^{\mathrm{UL}}|\mathbf{h}_{\mathrm{ER},k}|^2\right)^2}{4R_{\mathrm{ld},k}\eta_k^2 V_{\mathrm{T},k}^2} + \frac{\beta_k^2 R_{\mathrm{At},k}^3\left(\sum_{k=1}^{K}|\mathbf{h}_{\mathrm{e},k}\mathbf{p}_k|^2 + P_k^{\mathrm{UL}}|\mathbf{h}_{\mathrm{ER},k}|^2\right)^3}{32R_{\mathrm{ld},k}\eta_k^4 V_{\mathrm{T},k}^4} + \frac{\beta_k^2 R_{\mathrm{At},k}^4\left(\sum_{k=1}^{K}|\mathbf{h}_{\mathrm{e},k}\mathbf{p}_k|^2 + P_k^{\mathrm{UL}}|\mathbf{h}_{\mathrm{ER},k}|^2\right)^4}{1024R_{\mathrm{ld},k}\eta_k^6 V_{\mathrm{T},k}^6} \tag{3}$$

is the error variance. In this paper, σ_z^2 is not estimated but is assumed to be a fixed known value. In practice, this value is determined by the pilot SNR and training length from the pilot-based channel estimation stage (e.g., MMSE). Also, CSI reciprocity is assumed [8]. In order to achieve efficient WET and WIT communication, the spacing between the antenna elements at the FD-AP is considered large enough so that the small-scale fading between any two different antennas can be assumed to be independent [32], [33]. This assumption is extended to the antenna elements at FD-MUs, and a similar assumption holds for the reflection elements spacing of the RIS. Additionally, the total transmission period is T, which is fully used for the simultaneous WET and WIT transmissions.

With an assumed quasi-static flat-fading environment, the DL channels between; (i) the FD-AP and FD-MU k (i.e., $k = 1,\ldots,K$), (ii) the FD-AP and the RIS, and (iii) the RIS and the FD-MU k are denoted by $\mathbf{h}_{\mathrm{D},k} \in \mathbb{C}^{1\times M_{\mathrm{t}}}$, $\mathbf{H}_{\mathrm{D,R}} \in \mathbb{C}^{N\times M_{\mathrm{t}}}$ and $\mathbf{h}_{\mathrm{R},k} \in \mathbb{C}^{1\times N}$, respectively. The UL channels between; (i) the FD-MU k and FD-AP, (ii) the FD-MU k and RIS, and (iii) the RIS and the FD-AP are defined as $\mathbf{h}_{k,\mathrm{U}} \in \mathbb{C}^{M_{\mathrm{r}}\times 1} = \mathbf{h}_{\mathrm{D},k}^*$, $\mathbf{h}_{k,\mathrm{R}} \in \mathbb{C}^{N\times 1} = \mathbf{h}_{\mathrm{R},k}^*$, and $\mathbf{H}_{\mathrm{R,U}} \in \mathbb{C}^{M_{\mathrm{r}}\times N} = \mathbf{H}_{\mathrm{D,R}}^*$, respectively, due to channel reciprocity. The WP-IIoT network adopts the *harvest-then-transmit* protocol at the MUs. Furthermore, since both the FD-AP and FD-MUs experience SI, their interference channels are respectively defined as $\mathbf{H}_{\mathrm{AP}} \in \mathbb{C}^{M_{\mathrm{r}}\times M_{\mathrm{t}}}$ and $h_k \in \mathbb{C}^{1\times 1}$. Note, the SI at the MUs act as an extra source of RF energy scavenging termed as *energy-recycling* in this paper. Finally, co-channel interference (CoI) exists between the FD-MUs, and the CoI between FD-MU k and FD-MU j ($j \in \{1,\ldots,K\}$, $j \neq k$) is given as $h_{j,k} \in \mathbb{C}^{1\times 1}$. The FD-FD RIS-assisted WP-IIoT system details are presented next.

A. FD-FD System Signal Flow and Rate Formulation

During signal exchange in the FD-FD RIS-assisted IIoT network, both DL WET and UL WIT occur simultaneously. The DL WET and UL WIT are discussed as follows.

DL Energy harvesting: During the DL WET, MUs harvest energy transmitted from the FD-AP via direct and RIS cascaded links. Additionally, because of FD operational mode, the MUs harvest energy from the UL WIT signal, turning the negative SI signal into a positive energy scavenging signal, which we term as RF energy signal recycling. This implies that the FD-FD system harvests more energy compared to the existing FD-HD and HD-HD systems [8]. The DL WET signal received at FD-MU k from the FD-AP is given in (2), where P_j^{UL} is the transmit power of FD-MU j, and s_j^{UL} is the UL WIT

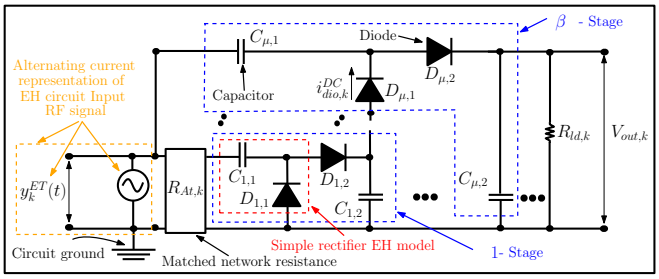

Fig. 2: Schematic diagram of EH circuit

signal transmitted to the FD-AP from the FD-MUs, where ($\mathbb{E}\{|s_j^{\mathrm{UL}}|^2\} = P_j^{\mathrm{UL}}$). The FD-AP transmitted signal to FD-MU k is defined as $\mathbb{E}\{|s_k^{\mathrm{DL}}|^2\} = 1$, and $\mathrm{n}_k^{\mathrm{DL}}$ is the antenna noise at FD-MU k and follows a complex Gaussian distribution with zero mean and noise variance, σ_k^2. The effective DL channel (i.e., direct + RIS cascaded link) of FD-MU k is defined as $\mathbf{h}_{\mathrm{e},k} = (\mathbf{h}_{\mathrm{R},k}\boldsymbol{\Phi}\mathbf{H}_{\mathrm{D,R}} + \mathbf{h}_{\mathrm{D},k})$. Also, the FD-AP DL beamformers and the RIS reflection co-efficient elements are defined as $\mathbf{p} = \{\mathbf{p}_k, k \in K\}$, $\boldsymbol{\Phi} = \mathrm{diag}(e^{j\phi_1}, e^{j\phi_2}, ..., e^{j\phi_N})$ and $\{\phi_n\}_{n=1}^{N} \in [\mathcal{F}_1]$, with $\mathcal{F}_1 = \{\phi_n |\ 0 \leq \phi_n \leq 2\pi\}$ denoting the set of continuous phase shift values [16]. The EH mathematical model adopted is the multi-stage rectifier non-linear EH model [29], [30], [34], which is based on the realistic simple rectifier EH model [35]–[37]. Moreover, the multi-stage rectifier non-linear EH model accounts for the received RF signal's slight *"amplification"* during DL WET by adopting a voltage multiplier within the EH circuitry [29], [30].

The equivalent circuit of a typical multi-stage rectifier EH model is shown in Fig. 2 Since each stage consists of 2 diodes and 2 capacitors, a β-stage rectifier has 2β diodes and 2β capacitors in total (i.e., multiple cascaded rectification and voltage boosting stages). Two equivalent circuits correspond to the RF signal and DC (0 Hz), respectively. RF power enters the input of the rectifier and is converted into DC at the output. At the RF frequency, capacitors can be simplified as short-circuited, so the 2β diodes are placed in parallel between input and output ports. Since the capacitors do not pass DC power, the 2β diodes are in series at 0 Hz. Using the EH model adopted, the generalized harvested energy at FD-MU k is derived and presented in (3), where $R_{\mathrm{At},k}$ is the antenna impedance load, $R_{\mathrm{ld},k}$ is the power management system load, $V_{\mathrm{T},k}$ is the diode thermal voltage, and η_k is the ideality factor respectively. In this paper, it is assumed that the SI components present at the FD-MU k contribute to the power harvested during WET in energy recycling. The multi-stage rectifier non-

$$\mathbf{y}_k^{\mathrm{UL}} = \underbrace{\sum_{k=1}^{K}(\mathbf{H}_{\mathrm{R,U}}\mathbf{\Phi}\mathbf{h}_{k,\mathrm{R}} + \mathbf{h}_{k,\mathrm{U}})\sqrt{P_k^{\mathrm{UL}}}s_k^{\mathrm{UL}}}_{\text{Signal from the FD-MUs}} + \underbrace{\hat{\mathbf{G}}\mathbf{x}^{\mathrm{DL}}}_{\text{Residual Self Interference}} + \underbrace{\mathbf{n}^{\mathrm{UL}}}_{\text{Noise}} \tag{4}$$

$$\hat{\mathrm{r}}_k^{\mathrm{UL}} = \mathbf{w}_k^H\mathbf{f}_{\mathrm{e},k}\sqrt{P_k^{\mathrm{UL}}}s_k^{\mathrm{UL}} + \mathbf{w}_k^H\sum_{j=1,j\neq k}^{K}\mathbf{f}_{\mathrm{e},j}\sqrt{P_j^{\mathrm{UL}}}s_j^{\mathrm{UL}} + \mathbf{w}_k^H\hat{\mathbf{G}}\sum_{j=1}^{K}\mathbf{p}_j s_j^{\mathrm{DL}} + \mathbf{w}_k^H\mathbf{n}^{\mathrm{UL}} \tag{5}$$

linear EH model derivation is presented in Appendix A.

UL Information transfer: During the UL WIT, the received signals from all the MUs is defined in (4), where the effective UL channel of FD-MU k is $\mathbf{f}_{\mathrm{e},k} = \left(\mathbf{H}_{\mathrm{R,U}}\mathbf{\Phi}\mathbf{h}_{k,\mathrm{R}} + \mathbf{h}_{k,\mathrm{U}}\right)$. The FD-AP uses the receive filter, $\mathbf{w}_k$, to detect the received signal from FD-MU k, where the decoded FD-MU k signal is mathematically defined in (5). The effective SI channel at the FD-AP is modeled as $\hat{\mathbf{G}} = \left(\mathbf{H}_{\mathrm{R,U}}\mathbf{\Phi}\mathbf{H}_{\mathrm{D,R}} + \mathbf{H}_{\mathrm{AP}}\right)$. Now, assuming the RIS elements phase shifts and $\hat{\mathbf{G}}$ are known at the FD-AP, the FD-AP applies SIC technique [8], [38] to detect the received data of MU k. However, the SIC technique is imperfect, meaning there is some residual SI (RSI) signal modeled as $\sigma_{\hat{G}}^2\|\mathbf{w}_k\|^2\sum_{j=1}^{K}\|\mathbf{p}_j\|^2$, having independent and identically distributed Gaussian components with zero mean and variance $\sigma_{\hat{G}}^2$. Note, in the instance where the RIS is co-located to the FD-AP, the SI at the FD-AP can be canceled by subtracting it from the UL received signal [15], [21], hence no RSI. Therefore, the UL rate of FD-MU k is expressed as

$$R_k^{\mathrm{UL}} = \log_2(1+\gamma_k^{\mathrm{UL}}), \tag{6}$$

with the signal-interference-noise-ratio (SINR) given as

$$\gamma_k^{\mathrm{UL}} = \frac{P_k^{\mathrm{UL}}|\mathbf{w}_k^H\mathbf{f}_{\mathrm{e},k}|^2}{\sum_{j\neq k}^{K}P_j^{\mathrm{UL}}|\mathbf{w}_k^H\mathbf{f}_{\mathrm{e},j}|^2 + \sum_{j=1}^{K}|\mathbf{w}_k^H\hat{\mathbf{G}}\mathbf{p}_j|^2 + \sigma_{\mathrm{AP}}^2\|\mathbf{w}_k^H\|^2}. \tag{7}$$

Sum-rate optimization problem: In this paper, the system sum-rate maximization problem is considered. The system sum-rate is maximized by joint design of the DL and UL transmission parameters, and the RIS passive beamformer, taking into account FD-AP and MUs power constraints. The system sum-rate maximization problem with respect to (w.r.t.) joint optimization of the associated variables $(\mathbf{p}_k, \mathbf{w}_k, \mathbf{\Phi}, P_k^{\mathrm{UL}})$ for the FD-FD RIS-assisted WP-IIoT system is formulated as

$$\begin{aligned}\underset{\mathbf{p}_k,\mathbf{\Phi},\mathbf{w}_k,P_k^{\mathrm{UL}}}{\text{maximize}} \sum_{k=1}^{K}R_k^{\mathrm{UL}} \text{ subject to } \sum_{k=1}^{K}\|\mathbf{p}_k\|^2 \leq P_{\max}^{\mathrm{DL}} \text{ (8a)},\\ P_k^{\mathrm{UL}} \leq \tilde{P}_k^{\mathrm{EH}}, \forall k \text{ (8b)}, \ \phi_n \in \mathcal{F}_1, \ \forall n \text{ (8c)},\end{aligned} \tag{8}$$

where $P_{\max}^{\mathrm{DL}}$ is the available power at the FD-AP. Constraint (8a) represents the DL transmit power budget which means the total allocated power for WET cannot exceed the maximum available power at the FD-AP. Constraint (8a) is a monotonically increasing function. The UL power budget of the MUs is also defined by constraint (8b), which is a monotonically increasing function. The power used for UL WIT should not exceed the total amount of power harvested. Finally, constraint (8c) ensures the phase shift of the nth reflector element lies within the range $\mathcal{F}_1$. It can be noted that the objective function of problem (8) is a non-convex optimization problem and challenging to solve due to the coupling of variables in the objective function [8], [38].

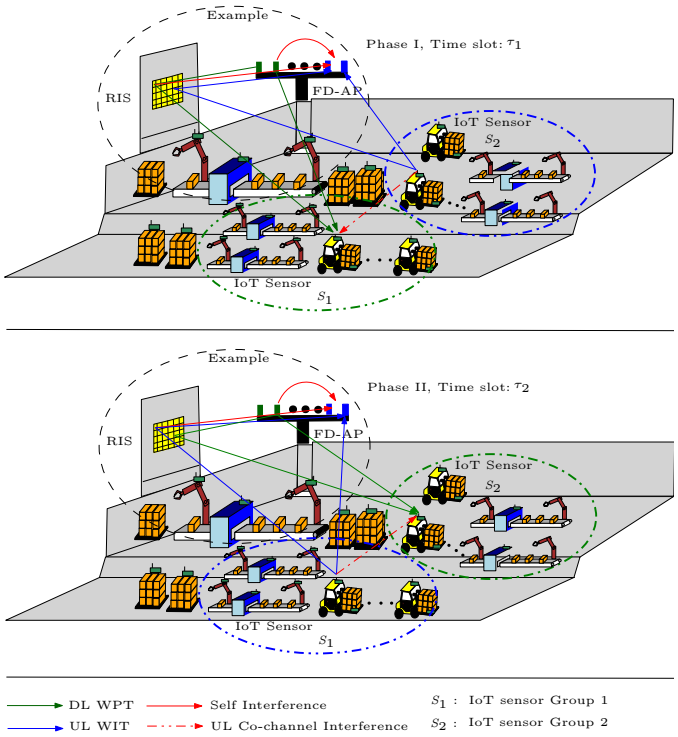

Fig. 3: FD-HD RIS-assisted WP-IIoT network system model.

B. Special Cases: FD-HD and HD-HD Systems

Here, the derivations of the FD-FD system model are extended to consider two special cases of the FD-FD RIS-assisted WP-IIoT network, which are used as benchmarks in this work. The two special cases considered are, namely, (i) FD-AP and two-user groups HD-MUs (FD-HD) [8], and (ii) HD-AP and HD-MUs (HD-HD) [8] RIS-assisted WP-IIoT network[3]. The benchmarks are discussed as follows.

FD-HD RIS-assisted WP-IIoT System: In this system setup as illustrated in Fig.3, the FD-AP operates in FD mode while the K MU IIoT sensor devices operate in HD mode. The K MU IIoT sensor devices are separated into two groups (i.e., HD-MUs) based on whether MUs are communicating in the DL or UL in time slot τ_l. The two groups are identified as, $\mathcal{S}_1$ group consisting of K_1 EH IIoT sensor devices which perform DL WET in phase 1 (τ_l) and UL WIT in phase 2 ($\tau_{\hat{l}}$). The second group, $\mathcal{S}_2$ is made up of K_2 EH IIoT sensor devices that perform UL WIT in phase 1 (τ_l) and DL WET in phase 2 ($\tau_{\hat{l}}$) [8]. For example, the first group $\mathcal{S}_1$ MUs perform DL EH in τ_1, while the second group $\mathcal{S}_2$ MUs send their UL messages to the FD-AP. Next, the first group $\mathcal{S}_1$ MUs perform UL communication in τ_2, while the second group $\mathcal{S}_2$ MUs

[3]Note that [8] does not consider RIS-assisted communication.

$$\mathrm{y}_{k,l}^{\mathrm{DL}} = \underbrace{\left(\mathbf{h}_{\mathrm{R},k,l}\boldsymbol{\Phi}\mathbf{H}_{\mathrm{D,R},l} + \mathbf{h}_{\mathrm{D},k,l}\right)\sum_{j\in S_l}^{K}\mathbf{p}_{j,l}s_{j,l}^{\mathrm{DL}}}_{\text{Energy signal}} + \underbrace{\sum_{jY\in S_{\hat{l}}}^{K}\left(\mathbf{h}_{j,\hat{l},\mathrm{R}}\boldsymbol{\Phi}\mathbf{h}_{\mathrm{R},k} + h_{j,\hat{l},k}\right)\sqrt{P_{j,\hat{l}}^{\mathrm{UL}}}s_{j,\hat{l}}^{\mathrm{UL}}}_{\text{UL co-channel interference}} + \underbrace{\mathrm{n}_k^{\mathrm{DL}}}_{\text{Noise}} \tag{9}$$

$$\tilde{P}_{k,l}^{\mathrm{EH}} = \frac{\tau_l\beta_k^2R_{\mathrm{At},k}^2\left(\sum_{j\in S_l}|\mathbf{h}_{\mathrm{e},kl}\mathbf{p}_{jl}|^2\right)^2}{4\tau_{\hat{l}}R_{\mathrm{ld},k}\eta_k^2V_{\mathrm{T},k}^2} + \frac{\tau_l\beta_k^2R_{\mathrm{At},k}^3\left(\sum_{j\in S_l}|\mathbf{h}_{\mathrm{e},kl}\mathbf{p}_{jl}|^2\right)^3}{32\tau_{\hat{l}}R_{\mathrm{ld},k}\eta_k^4V_{\mathrm{T},k}^4} + \frac{\tau_l\beta_k^2R_{\mathrm{At},k}^4\left(\sum_{j\in S_l}|\mathbf{h}_{\mathrm{e},kl}\mathbf{p}_{jl}|^2\right)^4}{1024\tau_{\hat{l}}R_{\mathrm{ld},k}\eta_k^6V_{\mathrm{T},k}^6} \tag{10}$$

$$\mathbf{y}_{k,\hat{l}}^{\mathrm{UL}} = \underbrace{\sum_{j\in S_{\hat{l}}}^{K}\left(\mathbf{H}_{\mathrm{R,U}}\boldsymbol{\Phi}\mathbf{h}_{j,\hat{l},\mathrm{R}} + \mathbf{h}_{j,\hat{l},\mathrm{U}}\right)\sqrt{P_{k,\hat{l}}^{\mathrm{UL}}}s_{k,\hat{l}}^{\mathrm{UL}}}_{\text{Signal from the FD-MUs}} + \underbrace{\hat{\mathbf{G}}_l\mathbf{x}^{\mathrm{DL}}}_{\text{Residual Self Interference}} + \underbrace{\mathbf{n}_{\mathrm{AP}}^{\mathrm{UL}}}_{\text{Noise}} \tag{11}$$

$$R_{k,l}^{\mathrm{UL}} = \sum_{l=1}^{2}a_{k,l}\tau_{\hat{l}}\log_2(1+\gamma_{k,l}^{\mathrm{UL}}),\ \gamma_{k,\hat{l}}^{\mathrm{UL}} = \frac{P_{k,\hat{l}}^{\mathrm{UL}}|\mathbf{w}_{k,\hat{l}}^H\hat{\mathbf{f}}_{k,\hat{l}}|^2}{\sum_{j\in S_{\hat{l}},j\neq k}^{K}P_{j,\hat{l}}^{\mathrm{UL}}|\mathbf{w}_{k,\hat{l}}^H\hat{\mathbf{f}}_{j,\hat{l}}|^2 + \sum_{j\in S_l}^{K}|\mathbf{w}_{k,\hat{l}}^H\hat{\mathbf{G}}_{\hat{l}}\mathbf{p}_{j,\hat{l}}|^2 + \sigma_{\mathrm{AP}}^2\|\mathbf{w}_{k,\hat{l}}^H\|^2} \tag{12}$$

undergo DL EH.

For simplicity, $K_1 = K_2 = K/2$. The HD-MUs communication occurs within the time periods τ_1 and τ_2. Also, due to the HD operation of the MUs, the HD-MUs do not experience SI, therefore, no energy recycling. The FD-HD RIS-assisted WP-IIoT system DL received signal, DL power harvested, UL receive signal, UL achievable rate, and UL achievable SNR are derived and presented in (9), (10), (11) and (12), respectively above, where $\hat{l} = 3 - l$, and $l = \{1, 2\}$ [8].

HD-HD RIS-assisted WP-IIoT System: In the HD-HD scenario, the system consists of an HD-AP and HD-MUs. Therefore, no MU groupings, CoI, and SI are present. Hence, the equations in this system scenario are similar to the FD-FD system without the MU groupings, no CoI, SI, and energy recycling components. The SINR and rate for the HD-HD system are derived, respectively, as

$$R_k^{\mathrm{UL}} = \tau_2\log_2(1+\gamma_k^{\mathrm{UL}}),\ \text{and} \tag{13}$$

$$\gamma_k^{\mathrm{UL}} = \frac{P_k^{\mathrm{UL}}|\mathbf{w}_k^H\hat{\mathbf{f}}_{\mathrm{e},k}|^2}{\sum_{j\neq k}^{K}P_j^{\mathrm{UL}}|\mathbf{w}_k^H\hat{\mathbf{f}}_{\mathrm{e},j}|^2 + \sigma_{\mathrm{AP}}^2\|\mathbf{w}_k^H\|^2}. \tag{14}$$

For the special cases system scenarios, the joint optimization problem w.r.t. the dependent variables is formulated as

$$\begin{aligned}
\underset{\tau_l,a_{k,l},\mathbf{p}_{k,l},\boldsymbol{\Phi},\mathbf{w}_{k,l},P_{k,\hat{l}}^{\mathrm{UL}}}{\text{maximize}}\ & \sum_{k=1}^{K}R_{k,\hat{l}}^{\mathrm{UL}}\ \text{subject to}\ P_{k,\hat{l}}^{\mathrm{UL}} \le \tilde{P}_{k,\hat{l}}^{\mathrm{EH}};\forall k\ \text{(15a)}\\
& \sum_{k=1}^{K}\sum_{l=1}^{2}\|\mathbf{p}_{k,l}\|^2 \le P_{\max}^{\mathrm{DL}}\ \text{(15b)}\\
& a_{k,l}\in\{0,1\},\ a_{k,1}+a_{k,2}=1;\forall k\ \text{(15c)}\\
& 0<\tau_l<1, \tau_1+\tau_2=1\ \text{(15d)}\\
& \phi_n\in\mathcal{F}_1,\ \forall n\ \text{(15e)}.
\end{aligned} \tag{15}$$

In Problem (15), the variables $a_{k,l}$ is a binary variable and determines the association of an MU to a transmission group, S_l at a given time for the FD-FD system, and its a non-convex constraint. For instance, when $a_{k,l} = 1$, this implies MU_k belongs to the EH group, S_1 in τ_1. The time allocation constraint for communication over the two phases is defined by (15d), which is a linear constraint. Constraint (15e) is the same as constraint (8c).

IV. Proposed Systems Optimization

In this section, solutions to Problems (8) and (15) are presented based on joint optimization of the various network resource variable. From the individual or isolated variables closed-form solutions, an alternating optimization algorithm is proposed to find the optimal resource variables that maximize the sum-rate. The solutions are presented as follows.

A. FD-FD System Sum-rate Maximization

Problem (8) is a non-convex optimization problem and hard to solve w.r.t all variables. Therefore, the problem is split into three main components, namely, the (i) RIS phase shift determination, (ii) the DL energy beamformer determination, and (iii) the other variables determination. The determination of components (i) and (ii) are easy and straight forward. However, sub-problem (iii) contains the sum-rate component which is still non-convex. Hence, the sum-rate-to-WMMSE equivalency approach is used to relax the problem and solve for the individual variables; P_k^{UL}, $\mathbf{p}_k$, $\mathbf{w}_k$ and $\boldsymbol{\Phi}$. Note that the WMMSE equivalent problem is convex with respect to each individual variable. Therefore, each variable is solved separately based on the WMMSE equivalent problem to find their closed-form solution. These closed-form solutions are adopted in an AO algorithm to acquire the optimal variables that maximize the system sum-rate.

***RIS phase shift determination*:** The optimal RIS phase shift design is obtained in closed-form as follows. From (6), the UL WIT achievable rate of the MU_k at the FD-AP is a monotonically increasing function w.r.t. $\|\mathbf{f}_{\mathrm{e},k}\|^2 = \|\mathbf{H}_{\mathrm{R,U}}\boldsymbol{\Phi}\mathbf{h}_{k,\mathrm{R}} + \mathbf{h}_{k,\mathrm{U}}\|^2$. Therefore, maximizing problem (8) w.r.t. $\boldsymbol{\Phi}$ is equivalent to the maximization of $\|\mathbf{f}_{\mathrm{e},k}\|^2$ [7], [17]. Hence, the RIS phase shift optimization problem is defined as[4]

$$\textbf{P1:}\ \underset{\boldsymbol{\Phi}}{\text{maximize}}\ \|\mathbf{H}_{\mathrm{R,U}}\boldsymbol{\Phi}\mathbf{h}_{k,\mathrm{R}} + \mathbf{h}_{k,\mathrm{U}}\|^2\ \text{subject to (8c).} \tag{16}$$

Due to the non-linear objective function and unit-modulus constraint on $\boldsymbol{\Phi}$, the problem is non-convex [7], [17]. By applying the change of variables to $\|\mathbf{H}_{\mathrm{R,U}}\boldsymbol{\Phi}\mathbf{h}_{k,\mathrm{R}} + \mathbf{h}_{k,\mathrm{U}}\|^2 = \|\mathbf{v}^H\boldsymbol{\Theta} + \mathbf{h}_{k,\mathrm{U}}\|^2$, where, $\mathbf{v} = [\nu_1, \nu_2, ..., \nu_N]^H = [e^{j\phi_1}, ..., e^{j\phi_N}]$, and

[4]Due to channel reciprocity, the optimal RIS phase shift obtained for UL WIT is the same for DL WET.

$\mathbf{\Theta} = \mathbf{H}_{\mathrm{R,U}}\mathrm{diag}(\mathbf{h}_{k,\mathrm{R}}) \in \mathbb{C}^{M\times N}$. Thus, using the triangular inequality, the upper bound of (16) is derived as

$$|\mathbf{v}^H\mathbf{\Theta} + \mathbf{h}_{k,\mathrm{U}}| \leq \sum_{n=1}^{N} |v_n[\mathbf{H}_{\mathrm{R,U}}]_{(:,n)}\mathbf{h}_{k,\mathrm{R}}[n]| + |\mathbf{h}_{k,\mathrm{U}}|, \quad (17)$$

With $\mathbf{g}_n \triangleq [\mathbf{H}_{\mathrm{R,U}}]_{(:,n)}\mathbf{h}_{k,\mathrm{R}}[n] \in \mathbb{C}^M$, problem **P1** becomes

$$\textbf{P1.1:} \underset{\phi_n}{\text{maximize}} \left\| \sum_{n=1}^{N} e^{j\phi_n}\mathbf{g}_n + \mathbf{h}_{k,\mathrm{U}} \right\|^2 \text{ subject to (8c).} \quad (18)$$

The objective function of (18) can be expanded as

$$\begin{aligned} &\left\| \sum_{n=1}^{N} e^{j\phi_n}\mathbf{g}_n + \mathbf{h}_{k,\mathrm{U}} \right\|^2 \\ &= \sum_{n=1}^{N} \|\mathbf{g}_n\|^2 + \|\mathbf{h}_{k,\mathrm{U}}\|^2 + 2\mathcal{R}e\left(\mathbf{h}_{k,U}^H \sum_{n=1}^{N} e^{j\phi_n}\mathbf{g}_n\right). \end{aligned} \quad (19)$$

Hence, to maximize the $\|\mathbf{f}_{\mathrm{e},k}\|^2$, the RIS phase shift of the nth reflecting element, ϕ_n is aligned with the direct uplink signal $\mathbf{h}_{k,\mathrm{U}}$. Adopting the optimal phase shift solution formulation approach in [17], the optimal phase shift of each RIS element should satisfy $e^{j\phi_n}\mathbf{g}_n = |\mathbf{g}_n|e^{\arg(\mathbf{h}_{k,\mathrm{U}}^H\mathbf{g}_n)}$. Thus, the optimal RIS phase shift of the nth reflection element, $\phi_n^\star$ is derived as

$$\phi_n^\star = -\arg(\mathbf{h}_{k,\mathrm{U}}^H\mathbf{g}_n), \quad (20)$$

where $\arg(\cdot)$ denotes the phase operator. Thus, the optimal phase shift matrix, $\mathbf{\Phi}^\star$ is derived from the phase shift vector, $\mathbf{v}$ as $\mathbf{\Phi}^\star = \mathrm{diag}(v_1, v_2, ..., v_N)$, where $v_n = e^{(-j\arg(\mathbf{h}_{k,\mathrm{U}}^H\mathbf{g}_n))}$. Therefore, through optimal phase shifts $\mathbf{\Phi}^\star$, the reflected and direct links between IIoT devices and AP are aligned.

***DL energy beamformer determination*:** The optimal DL energy beamformer is deduced from the Lagrangian duality approach. Based on Theorem 1 in [8], the optimal DL energy beamformer is deduced by differentiating the Lagrangian function of Problem (8) w.r.t $\mathbf{p}_k$ and using the Kuhn Tucker (KKT) conditions. The Lagrangian function of problem (8) over all variables and constraints is written as

$$\begin{aligned} \textbf{P2:}\ &\mathcal{L}(\mathbf{w}_k, \mathbf{p}_k, P_k^{\mathrm{UL}}, \lambda^{\mathrm{DL}}, \lambda_k^{\mathrm{UL}}, \mathbf{\Phi}) \\ &= \sum_{k=1}^{K} \log_2(1+\gamma_k^{\mathrm{UL}}) + \lambda^{\mathrm{DL}}P_{\max}^{\mathrm{DL}} - \sum_{k=1}^{K} \lambda_k^{\mathrm{UL}}P_k^{\mathrm{UL}} \\ &- \lambda^{\mathrm{DL}} \sum_{k=1}^{K} \|\mathbf{p}_k\|^2 + \sum_{k=1}^{K} \lambda_k^{\mathrm{UL}}\tilde{P}_k^{\mathrm{EH}}. \end{aligned} \quad (21)$$

From (21), the optimal $\mathbf{p}_k^\star$ for MU k is expressed as

$$\mathbf{p}_k^\star = \sqrt{P_{\max}^{\mathrm{DL}}}\mathbf{u}_{B,1}, \quad (22)$$

where $\mathbf{u}_{B,1}$ is the unit-norm of the dominant eigenvector corresponding to the maximum eigenvalue of matrix $B \triangleq \sum_{j=1}^{K} \lambda_j^{\mathrm{UL}}[(C_1) + (C_2)^2 + (C_3)^3)\hat{\mathbf{h}}_{\mathrm{e},j}\hat{\mathbf{h}}_{\mathrm{e},j}^H]$, where C_1, C_2 and C_3 are given as $\beta_k^2R_{\mathrm{At},k}^2/4R_{\mathrm{ld},k}\eta_k^2V_{\mathrm{T},k}^2$, $\beta_k^2R_{\mathrm{At},k}^3/32R_{\mathrm{ld},k}\eta_k^4V_{\mathrm{T},k}^4$ and $\beta_k^2R_{\mathrm{At},k}^4/1024R_{\mathrm{ld},k}\eta_k^6V_{\mathrm{T},k}^6$ respectively.[5] The optimal $\mathbf{p}_k$ solution is obtained by differentiating (21) and using the KKT conditions w.r.t $\mathbf{p}_k$. Hence, $\mathbf{p}_k$ is found from eigenvalue decomposition (EVD), and noting that the solution derived for the optimal $\mathbf{p}_k$ depends on the optimal λ^{DL} as follows.

The KKT conditions are given as

$$\mathbf{p}_k[\lambda_k^{\mathrm{UL}}(C_1+C_2+C_3)\mathbf{h}_{\mathrm{e},k}^H\mathbf{h}_{\mathrm{e},k} - 2\lambda^{\mathrm{DL}}\mathbf{I}_M] = 0, \quad (23)$$

$$\lambda^{\mathrm{DL}}\left(P_{\max}^{\mathrm{DL}} - \sum_{k=1}^{K}\|\mathbf{p}_k\|^2\right) = 0,\ \lambda_k^{\mathrm{UL}} \geq 0, \quad (24)$$

$$\sum_{k=1}^{K} \lambda_k^{\mathrm{UL}}\left(\tilde{P}_k^{\mathrm{EH}} - P_k^{\mathrm{UL}}\right) = 0, \text{ and } \lambda^{\mathrm{DL}} \geq 0. \quad (25)$$

From the KKT conditions, let denote $\mathbf{A} = \lambda_k^{\mathrm{UL}}(C_1+C_2+C_3)\mathbf{h}_{\mathrm{e},k}^H\mathbf{h}_{\mathrm{e},k} - 2\lambda^{\mathrm{UL}}\mathbf{I}_M$ and $\mathbf{B} = \lambda_k^{\mathrm{UL}}(C_1+C_2+C_3)\mathbf{h}_{\mathrm{e},k}^H\mathbf{h}_{\mathrm{e},k}$. When $\lambda^{\mathrm{DL}} = 0$, $\mathbf{A}\mathbf{p}_k = 0$ and $\lambda_k^{\mathrm{UL}} = 0$, then $-2\lambda^{\mathrm{DL}}\mathbf{I}_M = 0$, which contradicts the complementary slackness condition. If $\lambda^{\mathrm{DL}} > 0$ and $\lambda_K^{\mathrm{UL}} > 0$, then (23) satisfies the complementary slackness condition. Hence, λ^{DL} and $\lambda_k^{\mathrm{UL}} > 0$. From EVD of a matrix, $\mathbf{A}$ is decomposed as $\mathbf{A} = (\mathbf{U}_B\Lambda_B\mathbf{U}_B^H - 2\lambda^{\mathrm{UL}}\mathbf{I}_M)$, where $\mathbf{U}_B \in \mathbb{C}^{M\times M}$ is a unitary matrix with eigenvectors and $\Lambda_B = \mathrm{diag}(\lambda_{B,1}, ..., \lambda_{B,K})$ eigenvalues with $\lambda_{B,1} \geq \cdots \geq \lambda_{B,K}$. The optimal energy beamformer is solved for by multiplying through $(\mathbf{U}_B\Lambda_B\mathbf{U}_B^H - 2\lambda^{\mathrm{UL}}\mathbf{I}_M)\mathbf{p}_k = 0$ by $\mathbf{U}_B^H$ and solving for $\mathbf{p}_k$. Therefore, $\mathbf{p}_k$ is aligned with the dominant eigenvector of $\mathbf{B}$ corresponding to $\mathbf{u}_{B,1}$ which is a unit-norm eigenvector with the largest eigenvalue $\lambda_{B,1}$ (i.e., $\mathbf{A}\mathbf{u}_{B,1} = 0$). Hence, the optimal beamformer $\mathbf{p}_k^\star$ is presented in (22). Note that, the interference from both the direct and RIS reflected links is accounted for in $\mathbf{h}_{\mathrm{e}}$. Hence, from the derived optimal beamformer, $\mathbf{p}_k^\star$, the transmitted signal is projected in the direction that constructively aligns with the reflected links, thus avoiding interference.

***Other variables determination*:** From the sum-rate maximization problem in (8), the equivalent WMMSE minimization problem can be reformulated and deduced as [8]

$$\textbf{P3:} \underset{\mathbf{w}_k, \vartheta_k^{\mathrm{UL}}, P_k^{\mathrm{UL}}}{\text{minimize}} \sum_{k=1}^{K}(\vartheta_k^{\mathrm{UL}}e_k^{\mathrm{UL}} - \log\vartheta_k^{\mathrm{UL}}) \text{ subject to (8b),} \quad (26)$$

where, $\vartheta_k^{\mathrm{UL}}$ is the UL MMSE weight for MU_k and the MSE of the estimated signal at MU_k in UL-WIT is $e_k^{\mathrm{UL}} = \mathbb{E}\{(\hat{s}_k^{\mathrm{UL}} - s_k^{\mathrm{UL}})^H(\hat{s}_k^{\mathrm{UL}} - s_k^{\mathrm{UL}})\}$ and expanded as

$$\begin{aligned} e_k^{\mathrm{UL}} &= 1 - 2\mathcal{R}e\left\{\sqrt{P_k^{\mathrm{UL}}}\mathbf{w}_k^H\hat{\mathbf{f}}_{\mathrm{e},k}\right\} \\ &+ \sum_{j=1}^{K} P_j^{\mathrm{UL}}\mathbf{w}_k^H\hat{\mathbf{f}}_{\mathrm{e},j}\hat{\mathbf{f}}_{\mathrm{e},j}^H\mathbf{w}_k + \mathbf{w}_k^H\left(\sum_{j=1}^{K}\mathbf{p}_j^H\mathbf{p}_j\sigma_{\hat{G}}^2 + \sigma_{\mathrm{AP}}^2\right)\mathbf{w}_k. \end{aligned} \quad (27)$$

Now, Problem (26) is decomposed into single-variable subproblems with other variables fixed to find each variables optimal closed-form solution separately [8]. Specifically, the optimal receive filter, $\mathbf{w}_k^\star$ while fixing $\vartheta_k^{\mathrm{UL}}$ and P_k^{UL} is deduced

[5] Note that, $\mathbf{u}_{B,1}$ is obtained using the estimated channel $\hat{h}_{k,l}$ due to channel estimation and not the actual channel. The channel $\tilde{h}_{jl}$ is not used to determine $\mathbf{U}_{B,1}$.

from differentiating e_k^{UL} w.r.t $\mathbf{w}_k$ then equate to zero. Solving for $\mathbf{w}_k^{\star}$ from the differential is given as

$$\mathbf{w}_k^{\star} = \left(P_k^{\mathrm{UL}} \hat{\mathbf{f}}_{\mathrm{e},k}^H \hat{\mathbf{f}}_{\mathrm{e},k} + \sum_{j=1, j\neq k}^{K} P_k^{\mathrm{UL}} \hat{\mathbf{f}}_{\mathrm{e},j}^H \hat{\mathbf{f}}_{\mathrm{e},j} + c\mathbf{I}_M \right)^{-1} \sqrt{P_k^{\mathrm{UL}}} \hat{\mathbf{f}}_{\mathrm{e},k} \tag{28}$$

where, $c = (\sum_{j=1}^{K} \|\mathbf{p}_j\|^2 \sigma_{\hat{G}}^2 + \sigma_{\mathrm{AP}}^2) \|\mathbf{w}_k\|^2$. Next, the optimal UL MMSE weight, $\vartheta_k^{\mathrm{UL}}$ is found by differentiating the objective function in (26) w.r.t $\vartheta_k^{\mathrm{UL}}$, equating to zero and solving for $\vartheta_k^{\mathrm{UL}\star}$, which is derived as

$$\vartheta_k^{\mathrm{UL}\star} = \frac{1}{1 - \sqrt{P_k^{\mathrm{UL}}} \mathbf{w}_k^H \hat{\mathbf{f}}_{\mathrm{e},k}} \tag{29}$$

By simplifying and grouping like terms of the objective function in Problem (26) w.r.t. P_k^{UL}, the expression for equation components associated with P_k^{UL} and other variables is denoted as Ω^{UL}, and obtained as

$$\Omega^{\mathrm{UL}} = \sum_{k=1}^{K} \Bigg[\vartheta_k^{\mathrm{UL}} \left(\sum_{j=1}^{K} \|\mathbf{p}_j\|^2 \hat{\sigma}_{\hat{G}}^2 + \sigma_{\mathrm{AP}}^2 \right) \|\mathbf{w}_k\|^2 + \vartheta_k^{\mathrm{UL}} - \log \vartheta_k^{\mathrm{UL}} + \sum_{j=1}^{K} \vartheta_k^{\mathrm{UL}} P_j^{\mathrm{UL}} |\mathbf{w}_k^H \hat{\mathbf{f}}_{\mathrm{e},j}|^2 - \sqrt{P_k^{\mathrm{UL}}} \vartheta_k^{\mathrm{UL}} (\mathbf{w}_k^H \hat{\mathbf{f}}_{\mathrm{e},k} + \hat{\mathbf{f}}_{\mathrm{e},k}^H \mathbf{w}_j) \Bigg]. \tag{30}$$

This implies that the optimal UL transmit power of MU_k is deduced by considering the terms in (30) associated with only P_k^{UL} and denoting as

$$\Theta = \sum_{k=1}^{K} \left[\vartheta_k^{\mathrm{UL}} \sum_{j=1}^{K} P_j^{\mathrm{UL}} |\mathbf{w}_k^H \hat{\mathbf{f}}_{\mathrm{e},j}|^2 - \sqrt{P_k^{\mathrm{UL}}} \vartheta_k^{\mathrm{UL}} (\mathbf{w}_k^H \hat{\mathbf{f}}_{\mathrm{e},k} + \hat{\mathbf{f}}_{\mathrm{e},k}^H \mathbf{w}_j) \right]. \tag{31}$$

the optimization problem for finding the optimal UL power, $P_k^{\mathrm{UL}\star}$ is written as

$$\underset{P_k^{\mathrm{UL}}}{\text{minimize}}\ \Theta \text{ subject to (8b)}. \tag{32}$$

From the Lagrangian function written as

$$\mathcal{L}(P_k^{\mathrm{UL}}, \lambda_k^{\mathrm{UL}}) = \lambda_k^{\mathrm{UL}} (P_k^{\mathrm{UL}} - \tilde{P}_k^{\mathrm{EH}}) + \sum_{k=1}^{K} \Bigg(\vartheta_k^{\mathrm{UL}} \sum_{j=1}^{K} P_j^{\mathrm{UL}} |\mathbf{w}_k^H \hat{\mathbf{f}}_{\mathrm{e},j}|^2 - \sqrt{P_k^{\mathrm{UL}}} \vartheta_k^{\mathrm{UL}} (\mathbf{w}_k^H \hat{\mathbf{f}}_{\mathrm{e},k} + \hat{\mathbf{f}}_{\mathrm{e},k}^H \mathbf{w}_j^H) \Bigg), \tag{33}$$

the optimal UL power allocation $P_k^{\mathrm{UL}\star}$ is found by differentiating (33) and equating to zero and finding P_k^{UL}. The optimal UL power allocation, $P_k^{\mathrm{UL}\star}$ is deduced as

$$P_k^{\mathrm{UL}\star} = \left(\frac{\vartheta_k^{\mathrm{UL}} \mathbf{w}_k^H \hat{\mathbf{f}}_{\mathrm{e},k}}{\sum_{j=1}^{K} \vartheta_j^{\mathrm{UL}} |\mathbf{w}_k^H \hat{\mathbf{f}}_{\mathrm{e},k}|^2 - \lambda_k^{\mathrm{UL}}} \right)^2. \tag{34}$$

Next, the UL power budget of MU_k is satisfied by solving for λ_k^{UL}. By substituting (34) into the power budget constraint in (8b), λ_k^{UL} is expressed as

$$\lambda_k^{\mathrm{UL}} = \sum_{j=1}^{K} \vartheta_j^{\mathrm{UL}} |\mathbf{w}_j^H \hat{\mathbf{f}}_{\mathrm{e},k}|^2 - \frac{\vartheta_k^{\mathrm{UL}} \mathbf{w}_k^H \hat{\mathbf{f}}_{\mathrm{e},k}}{\sqrt{\tilde{P}_k^{\mathrm{EH}}}}. \tag{35}$$

The AO algorithm for determining the maximum system sum-rate is presented in Algorithm 1.

Algorithm 1 FD-FD: Sum-Rate Optimization Scheme

1: Determine the RIS phase-shift $\{\phi_n\}$ using (20).
2: **Initialize**: λ_k^{UL} and P_k^{UL}.
3: **repeat**
4: **for** each mobile user k **do**
5: Update $\{\mathbf{p}_k\}$, $\{\mathbf{w}_k\}$, $\{\vartheta_k^{\mathrm{UL}}\}$ from (22), (28), (29).
6: Update $\{\lambda_k^{\mathrm{UL}}\}$, $\{P_k^{\mathrm{UL}}\}$ according to (35), (34).
7: **end for**
8: **until** The objective function of Problem (8) converges.

Algorithm 2 FD/HD-HD: Sum-Rate Optimization Scheme

1: Determine the RIS phase-shift $\{\phi_{n,\hat{l}}\}$ using (36).
2: **Initialize**: $\lambda_{k,l}^{\mathrm{UL}}$, $P_{k,l}^{\mathrm{UL}}$, and τ_l
3: **repeat**
4: **repeat**
5: **for** each mobile user k **do**
6: Update $\{\mathbf{p}_{k,l}\}$, $\{\mathbf{w}_{k,\hat{l}}\}$ using (37), (43)
7: Update $\{\vartheta_{k,\hat{l}}^{\mathrm{UL}}\}$, $\{\lambda_{k,l}^{\mathrm{UL}}\}$ according to (38), (40).
8: Update $\{P_{k,l}^{\mathrm{UL}}\}$ according to (39).
9: **if** FD-HD **then**
10: Update $\{a_{k,l}\}$ and $\{a_{k,\hat{l}}\}$ using BBA [8]
11: **else**
12: For HD-HD: $\{a_{k,l}\} = 1$ and $\{a_{k,\hat{l}}\} = 0$
13: **end if**
14: **end for**
15: **until** Sum-rate (15) converges with fixed $\{\tau_l\}$.
16: Update $\{\tau_l\}$ with Golden Line Search method.
17: **until** convergence.

B. Special Cases Sum-rate Maximization

FD-HD System Sum-rate Maximization: The formulated optimization problem (15) is a non-convex mixed-integer programming problem when jointly optimizing all variables [8]. The only difference between the special case FD-HD system and the system presented in [8] is the introduction of the RIS. Hence, the solution and derivation steps for our benchmark are the same as in [8] but with the RIS component adding a cascade channel within each closed-form solution. Additionally, the optimal RIS phase shift is determined in our benchmark, while it is not determined in [8]. Therefore, the closed-form individual variables solutions are presented as follows, with its associated AO algorithm presented in Algorithm 2.

Here, the solutions to the optimal RIS phase shift and the DL energy beamformer are derived and have similar solutions in (20) and (22), respectively. The RIS phase shift and the DL energy beamformer are respectively deduced as

$$\phi_{n,\hat{l}}^{\star} = -\arg(\mathbf{h}_{k,\mathrm{U}}^H \mathbf{g}_n), \text{ and} \tag{36}$$

$$\mathbf{p}_{k,l}^{\star} = \sqrt{P_{\max}^{\mathrm{DL}}} \mathbf{u}_{B,1}, \tag{37}$$

Similarly, the derivation of the other variables follows the same sum-rate-to-WMMSE conversion. With the exception of the user grouping and time allocation, the other variables are solved using the same approach. Therefore, the receive filter,

TABLE IV: Comparison of computational complexity and overhead costs.

Scheme	Computational Complexity	Overhead Cost
Proposed FD-FD	$O\left(N + I_T\left[K^8 + \log(1/\epsilon_T)\right]\right)$	$K(i_o + B) + F$
FD-HD	$O(N + I_O\left[I_T\left[2^9K^9 + \log(1/\epsilon_T)\right] + K + \log(1/\epsilon_O)\right])$	$K(i_o + 2B) + F$
HD-HD	$O(N + I_O\left[I_T\left[K^9 + \log(1/\epsilon_T)\right] + K + \log(1/\epsilon_O)\right])$	$K(i_o + B) + F$

UL power allocation, and UL Lagrangian are respectively derived as

$$\vartheta_{k,l}^{\mathrm{UL}\star} = \frac{1}{1 - \sqrt{P_{k,l}^{\mathrm{UL}}}\mathbf{w}_{k,l}^H\hat{\mathbf{f}}_{\mathrm{e},kl}}, \tag{38}$$

$$P_{k,l}^{\mathrm{UL}\star} = \left(\frac{a_{k,\hat{l}}\vartheta_{k,l}^{\mathrm{UL}}\mathbf{w}_{k,l}^H\hat{\mathbf{f}}_{\mathrm{e},kl}}{\sum_{j=1}^{\mathcal{S}_{\hat{l}}} a_{j,\hat{l}}\vartheta_{j,l}^{\mathrm{UL}}|\mathbf{w}_{j,l}^H\hat{\mathbf{f}}_{\mathrm{e},kl}|^2 - \lambda_k^{\mathrm{UL}}}\right)^2, \tag{39}$$

and

$$\lambda_k^{\mathrm{UL}} = \sum_{j=1}^{\mathcal{S}_{\hat{l}}} a_{j,\hat{l}}\vartheta_{j,l}^{\mathrm{UL}}|\mathbf{w}_{j,l}^H\hat{\mathbf{f}}_{\mathrm{e},kl}|^2 - \frac{a_{k,\hat{l}}\vartheta_{k,l}^{\mathrm{UL}}\mathbf{w}_{k,l}^H\hat{\mathbf{f}}_{\mathrm{e},kl}}{\sum_{l=1}^{2}\sqrt{\tilde{P}_{k,l}^{\mathrm{EH}}}}, \tag{40}$$

The user grouping problem is a mixed integer linear programming (MILP) problem given as

$$\underset{a_{k,l}}{\text{minimize}} \sum_{k=1}^{K} R_{k,l}^{\mathrm{UL}} \text{ subject to } \sum_{l=1}^{2} a_{k,l} = 1, a_{k,l} \in \{0,1\}. \tag{41}$$

This problem is non-convex but can be solved using the branch-and-bound approach (BBA) employed in [8].

The optimal time allocation, $\tau_l^\star$, is solved by considering the optimization problem expressed as

$$\underset{\tau_l}{\text{maximize}} \sum_{k=1}^{K} R_{k,l}^{\mathrm{UL}} \text{ subject to (15d).} \tag{42}$$

Problem (42) is convex, a simple golden line search method (GLSM) can be used to obtain the optimal, $\tau_l^\star$ [8].

HD-HD System Sum-rate Maximization: The FD-HD system optimal closed-form solutions for $\mathbf{p}_{k,l}^{\mathrm{UL}\star}, P_{k,l}^{\mathrm{UL}\star}, \vartheta_{k,l}^{\mathrm{UL}\star}$, $\tau_l^\star$ and $\mathbf{\Phi}^\star$ are reused for the HD-HD system [8]. However, due to the absence of RSI in the HD-HD system, the solution for $\mathbf{w}_{k,l}^\star$ is modified as

$$\mathbf{w}_{k,l}^\star = \left(\sum_{j\in\mathcal{S}_{\hat{l}}} P_{j,l}^{\mathrm{UL}}\hat{\mathbf{f}}_{\mathrm{e},jl}\hat{\mathbf{f}}_{\mathrm{e},jl}^H + \sigma_l^2\mathbf{I}_M\right)^{-1}\sqrt{P_{k,l}^{\mathrm{UL}}}\hat{\mathbf{f}}_{\mathrm{e},kl}, \tag{43}$$

Note, in the HD-HD system, all MUs are in the same group and perform DL WET in phase 1 and UL WIT in phase 2.

C. Computational Complexity and Overhead Analysis

Here, the complexity of the algorithms proposed is discussed. Note that the convexity and convergence for FD-FD, FD-HD, and HD-HD are similar to those presented in [8]. Therefore, for brevity and reduced repetition, the convexity and convergence proof are not presented in this paper, but can be inferred from [8]. Algorithm 1 and 2 are implemented centrally at the AP and determine all the optimal variables, including the transmit power, $\{P_k^{\mathrm{UL}}\}_{k=1}^K$ of MUs. For Algorithm 1 and 2, the Big O computational complexity for solving (8) and (15) are $O\left(N + I_T\left[K^8 + \log(1/\epsilon_T)\right]\right)$ and $O(N + I_O\left[I_T\left[2^9K^9 + \log(1/\epsilon_T)\right] + K + \log(1/\epsilon_O)\right])$, respectively, where I_T and I_O denote the computations of iterations of Algorithm 1 and 2, respectively, to converge. ϵ_T and ϵ_O are the convergence criterion for both Algorithms, respectively, and K represents the sum-rate calculation in the GLSM used for determining the time-slots. The total arithmetic computations in the FD-FD system for all variables $\{\phi_n\}_{n=1}^N$, $\{\mathbf{p}_k\}_{k=1}^K$, $\{\mathbf{w}_k\}_{k=1}^K$, $\{\vartheta_k^{\mathrm{UL}}\}_{k=1}^K$, $\{\lambda_k^{\mathrm{UL}}\}_{k=1}^K$ and $P_k^{\mathrm{UL}}\}_{k=1}^K$ and the sum-rate convergence calculation is K^8. In the FD-HD system, the computations for all variables $\{\phi_{n,\hat{l}}\}_{n=1,l=1}^{N,2}$, $\{\mathbf{p}_{k,l}\}_{k=1,l=1}^{K,2}$, $\{\mathbf{w}_{k,\hat{l}}\}_{k=1,l=1}^{K,2}$, $\{\vartheta_{k,\hat{l}}^{\mathrm{UL}}\}_{k=1,l=1}^{K,2}$, $\{\lambda_{k,l}^{\mathrm{UL}}\}_{k=1,l=1}^{K,2}$, $\{P_{k,l}^{\mathrm{UL}}\}_{k=1,l=1}^{K,2}$, $\{a_{k,l}\}_{k=1,l=1}^{K,2}$ and the sum-rate convergence and $\{\tau_l\}$ is 2^9K^9. For the HD-HD system, the MUs are in a single group and therefore have an arithmetic computation of all variables as K^9, while the calculations for the number of elements in all three systems are N.

The number of bits to transmit $\{P_k^{\mathrm{UL}}\}_{k=1}^K$ to MUs in the FD-FD system is $K(i_o + B) + F$, and $K(i_o + 2B) + F$ in both FD-HD and HD-HD systems, where i_o, B and F are the number of index bits of MUs, real numbers bits, and information bits, respectively. From both algorithms presented, it can be deduced that Algorithm 1 for optimizing the FD-FD system has the least computational complexity and overhead, while Algorithm 2 for optimizing HD-HD system has a moderate and slightly modified computational complexity given as $O(N + I_O\left[I_T\left[K^9 + \log(1/\epsilon_T)\right] + K + \log(1/\epsilon_O)\right])$ since this system has no user groupings. Algorithm 2, also for optimizing the FD-HD system, has the highest computational complexity in this case. Both FD-FD and HD-HD have the same overhead cost. The computational complexity and overhead cost for the three schemes are summarized in Table IV.

However, to mitigate the complexity of Algorithms 1 and 2, a staggered (Stg) partial-update variant, updating disjoint variable blocks in alternation, is introduced [29], together with a benchmark maximum ratio combining (MRC) scheme for comparison. Stg updates only a subset of the problem variable blocks per iteration, while the remaining blocks are left unchanged for that iteration. The Stg approach offers a reduced computational burden as $O(N + I_T\left[K^x + \log(1/\epsilon_O)\right])$ for FD-FD system, and $O(N + I_O\left[I_T\left[2^xK^x + \log(1/\epsilon_T)\right] + K + \log(1/\epsilon_O)\right])$, and $O(N + I_O\left[I_T\left[K^x + \log(1/\epsilon_T)\right] + K + \log(1/\epsilon_O)\right])$ for FD-HD and HD-HD respectively, with $x(\leq 9)$ denoting the number of variables updated per iterations [29]. The MRC baseline scheme is non-iterative, hence has a very low complexity given as $O(N + K^2)$.

V. Numerical Evaluation and Discussion

This section presents performance simulations on the proposed FD-FD RIS-assisted WP-IIoT system. The system parameters used in the simulation are summarized in Table V.

TABLE V: Simulation variable definitions and values.

Variable	Values	Variable	Values	Variable	Values
$\kappa_{\mathrm{DL}}, \kappa_{\mathrm{DL},k}$	10 dB	K	6	η_k	1.05
$M_{\mathrm{t}}, M_{\mathrm{r}}$	10	N	60	$\sigma^2_{\tilde{G}}$	-110 dBm
τ_1, τ_2	0.5	β_k	4	σ^2_{AP}	-96 dBm
$R_{\mathrm{At},k}$	50Ω	$R_{\mathrm{Ld},k}$	100kΩ	$V_{\mathrm{T},k}$	25.86 mV

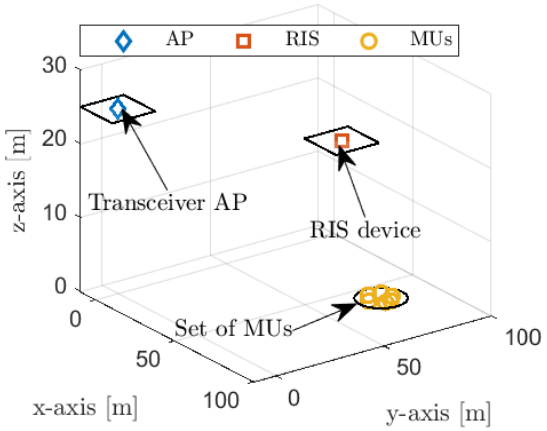

Fig. 4: Example of simulated system topology.

TABLE VI: Scenarios and cases definitions.

Case	Proposed FD-FD	FD-HD [8]	HD-HD [8]
With RIS	FF-WR	FH-WR	HH-WR
No RIS	FF-NR	FH-NR	HH-NR

An example of the simulation topology is shown in Fig. 4, where the FD-AP and the RIS are located at (0,0,25)m and (60,60,22.5)m respectively. The FD-MUs are randomly deployed within a circular area centered at (80,0) with a radius of 5m and height 1.5m. We set signal attenuation at -10 dB, and assume a pathloss exponent of 2.5 between the AP-RIS and RIS-MUs channels, and 2.9 between the AP-MUs channel [7]. We compare two benchmarks, namely, the FD-HD and the HD-HD systems to the proposed FD-FD system. In addition, the cases of RIS present or absent are considered for all scenarios. The combination of the scenarios with the cases are defined in Table VI. The results presented were obtained from running 10^4 random channel realizations.

Now, the proposed network communication channels are modeled as follows. The large-scale fading channels are modeled as $\sqrt{A_0(d/d_0)^{-}\alpha}$, where A_0, d_0, d and α are the signal attenuation value, reference distance of 1m, the inter-device distance, and the pathloss exponent, respectively. $\mathbf{h}_{\mathrm{D},k}$ and $\mathbf{h}_{k,\mathrm{U}} = \mathbf{h}^*_{\mathrm{D},k}$ are the AP-MU direct link small-scale fading components modeled as Rayleigh fading channels with $\mathcal{CN}(0,1)$ [7]. The AP-RIS and RIS-MU small-scale fading channels components are modeled as Rician fading channels and given as $\mathbf{H}_{\mathrm{R,U}} = \mathbf{H}^*_{\mathrm{D,R}}$, $\mathbf{h}_{k,\mathrm{R}} = \mathbf{h}^*_{\mathrm{R},k}$, with

$$\mathbf{H}_{\mathrm{D,R}} = \sqrt{\epsilon_{\mathrm{DL}}}\left(\sqrt{\frac{\kappa_{\mathrm{DL}}}{\kappa_{\mathrm{DL}}+1}}\bar{\mathbf{H}}_{\mathrm{D,R}} + \sqrt{\frac{1}{\kappa_{\mathrm{DL}}+1}}\tilde{\mathbf{H}}_{\mathrm{D,R}}\right), \tag{44}$$

$$\mathbf{h}_{\mathrm{R},k} = \sqrt{\epsilon_{\mathrm{DL},k}}\left(\sqrt{\frac{\kappa_{\mathrm{DL},k}}{\kappa_{\mathrm{DL},k}+1}}\bar{\mathbf{h}}_{\mathrm{R},k} + \sqrt{\frac{1}{\kappa_{\mathrm{DL},k}+1}}\tilde{\mathbf{h}}_{\mathrm{R},k}\right) \tag{45}$$

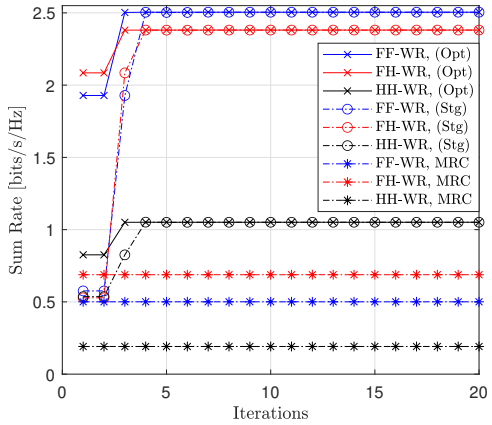

Fig. 5: Convergence of proposed algorithms for $P^{\mathrm{DL}}_{\max}$10 dB.

where ϵ_{DL} and $\epsilon_{\mathrm{DL},k}$ are the distance-dependent pathloss of AP to RIS, and RIS to FD-MU k respectively, and κ_{DL}, and $\kappa_{\mathrm{DL},k}$ are the Rician factors [7]. $\tilde{\mathbf{H}}_{\mathrm{D,R}}$ and $\tilde{\mathbf{h}}_{\mathrm{R},k}$ are the non-line-of-sight (NLoS) scattering components with their elements distributed as i.i.d complex Gaussian with zero mean and unit variance. The line-of-sight (LoS) components are expressed using the uniform linear array (ULA) as;

$$\mathbf{a}_N(\theta) = [1, e^{j2\pi\frac{d}{\lambda}\sin\theta}, ..., e^{j2\pi\frac{d}{\lambda}(N-1)\sin\theta}], \tag{46}$$

where θ is the angle of departure (AoD) at the FD-AP, or the angle of arrival (AoA) at the RIS. d and λ are the element spacing and signal wavelength. $\bar{\mathbf{H}}_{\mathrm{D,R}}$ and $\bar{\mathbf{h}}_{\mathrm{R},k}$ are respectively expressed as;

$$\bar{\mathbf{H}}_{\mathrm{D,R}}(\theta) = \mathbf{a}^H_N(\theta_{\mathrm{AoA},1})\mathbf{a}_{M_t}(\theta_{\mathrm{AoD},1}), \text{ and } \bar{\mathbf{h}}_{\mathrm{R},k}(\theta) = \mathbf{a}_N(\theta_{\mathrm{AoD},2}), \tag{47}$$

where $\theta_{\mathrm{AoD},1}$ is the AoD from the ULA at the FD-AP, and $\theta_{\mathrm{AoA},1}$ is the AoA at the ULA at the RIS. Similarly, $\theta_{\mathrm{AoD},2}$ is the AoD of FD-MU k at the RIS. It is important to note that adopting the standard Rayleigh/Rician models in IIoT scenarios is reasonable, as they jointly capture the rich scattering and strong LoS components. In IIoT settings, the environment is characterized by several metallic machines and reflective surfaces that produce severe multipath and frequent shadowing. In such a harsh industrial environment, IoT devices cannot be deployed without LoS, hence, it is appropriate to adopt Rayleigh/Rician models [39].

A. Simulation Results and Discussion

Performance of Proposed Algorithm: The convergence behavior of the proposed algorithm, and the new variant is presented in Fig. 5, including the MRC scheme as a baseline for comparison. As shown in Fig. 5, the proposed optimized (Opt) scheme and the Stg converge to similar sum-rate values. However, Opt achieves faster convergence with very few iterations. Although Stg distributes its computational load in blocks across each iteration, it requires a few additional iterations for convergence. The MRC baseline is non-iterative, hence appears as a constant curve across iterations. It attains a lower sum-rate because it does not actively suppress MU interference or RSI, but it provides a useful low-complexity.

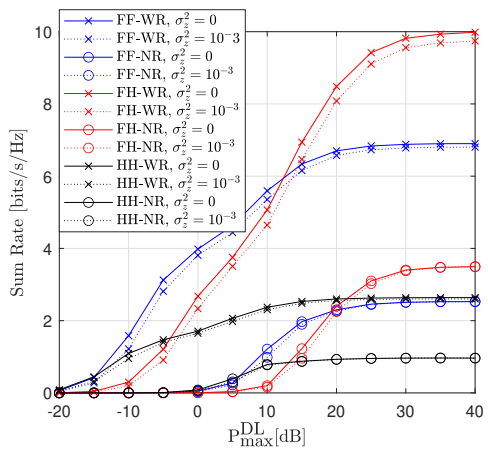

(a) Sum-rate vs P^{DL}_{max}.

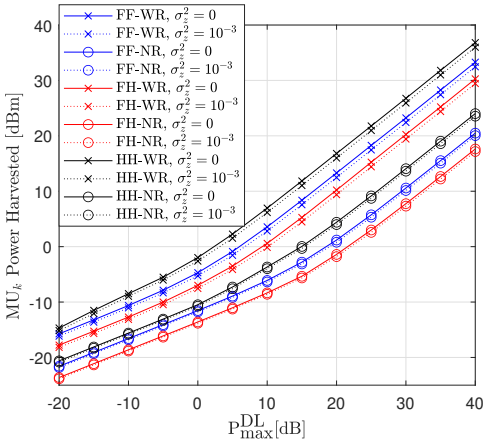

(b) MU_k harvested power vs P^{DL}_{max}.

Fig. 6: Effects of AP transmit power on system performance.

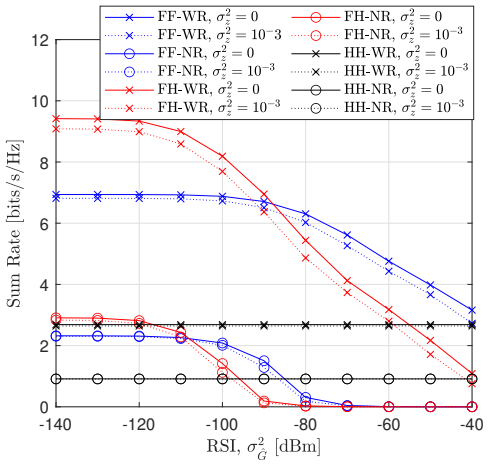

(a) Sum-rate vs RSI ($\sigma^2_{\hat{G}}$).

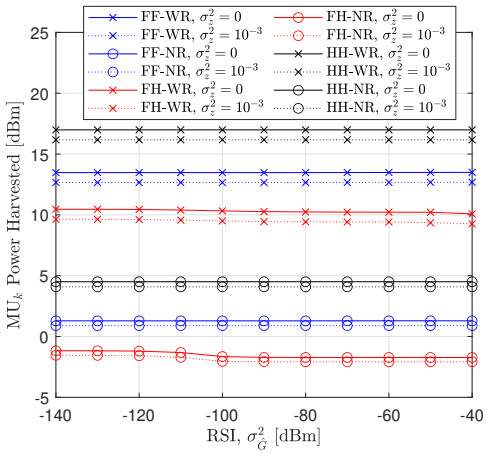

(b) MU_k harvested power vs RSI ($\sigma^2_{\hat{G}}$).

Fig. 7: Effects of RSI on system performance.

Fig. 6 shows the influence of the AP transmit power, P^{DL}_{max}, on the system. As shown in Fig. 6a, the system sum-rate for all three systems improves with increasing P^{DL}_{max}. This is because MUs harvest more energy when P^{DL}_{max} increases, as seen in Fig. 6b. However, the sum-rate for all schemes attain saturation due to increased interference from other MUs due to UL transmission. It can be observed that in the low P^{DL}_{max} regime ($-20 < P^{DL}_{max} < 12$) dB, the FF-WR system outperforms both the FH-WR and the HH-WR systems due to the HD and time splits components. When $P^{DL}_{max} < -5$ dB, the HH-WR system is seen to outperform the FH-WR system. This behavior is due to the dominant effect of the RSI in the FH-WR system. At $P^{DL}_{max} > 12$ dB region, the FH-WR system shows an increase in system performance compared to the FF-WR due to the larger MUs and RSI interference signal strength in the FF-WR system. The FH-WR system suffers from $K/2$ interfering signals from other MUs during UL WIT, while the FF-WR system is affected by $K-1$ interfering signals during UL WIT. For example, at $P^{DL}_{max} = 30$ dB, the FH-WR system achieves approximately 3 bps/s/Hz sum-rate gain over the FF-WR system, and approximately 6 bps/s/Hz over its FH-NR counterpart. The NR scenarios have a similar behavior to the discussed WR scenarios. The results also show the impact of channel imperfections based on channel error factor, σ_z^2. With $\sigma_z^2 = 10^{-3}$, the sum-rate reduces marginally due to increase in error during channel estimation. Fig. 6b shows that the WR systems yield higher harvested power because of energy beamforming diversity gain from the RIS. As P^{DL}_{max} increases, the total power harvested by each MU_k increases. HH systems slightly harvest more power (approximately 0.1 dBm at $P^{DL}_{max} = 30$ dB) than the FH and FF systems due to no effective SI suppression in determining the DL energy beamformer $\mathbf{p}_k$, as done for the FD systems which affects the power harvesting performance. FF-WR system is observed to harvest slightly more energy than the FH-WR system due to the recycled channel.

In Fig. 7, the effect of RSI power/variance on system performance is shown. It is evident that as the overall RSI power ($\sigma^2_{\hat{G}}$) increases, the sum-rate for the FD systems reduces. This is due to the increase in RSI power occurring at the AP, meaning there is a higher SI effect. In the low $\sigma^2_{\hat{G}}$ regime ($\sigma^2_{\hat{G}} < -90$ dBm), the FH-WR system shows superior performance (i.e., approximately 2.1 bps/s/Hz, at $\sigma^2_{\hat{G}} = -120$ dBm) in sum-rate gain over the FF-WR system. This is due to the FH-WR having less MUs' interference compared to the FF-WR at the high AP transmit power and fewer users per group. In the high $\sigma^2_{\hat{G}}$ regime ($-90 > \sigma^2_{\hat{G}} < -40$) dBm,

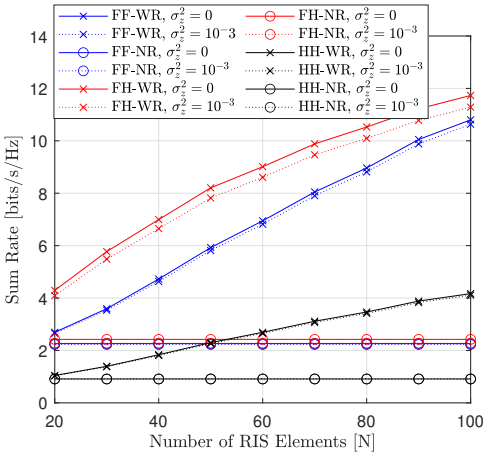

(a) Sum-rate vs N.

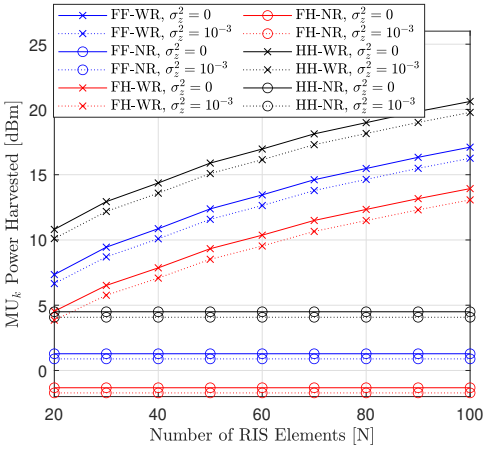

(b) MU_k harvested power vs N.

Fig. 8: Effects of RIS elements on system performance.

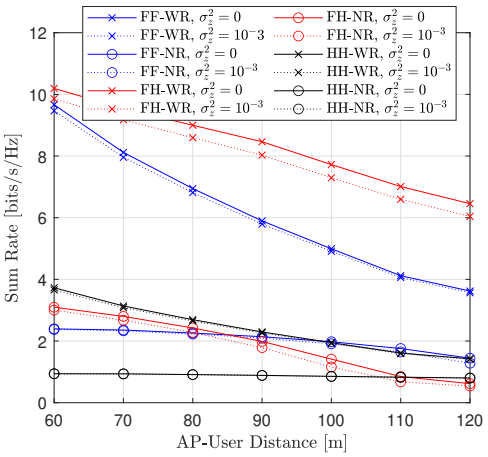

(a) Sum-rate vs AP-User distance [m].

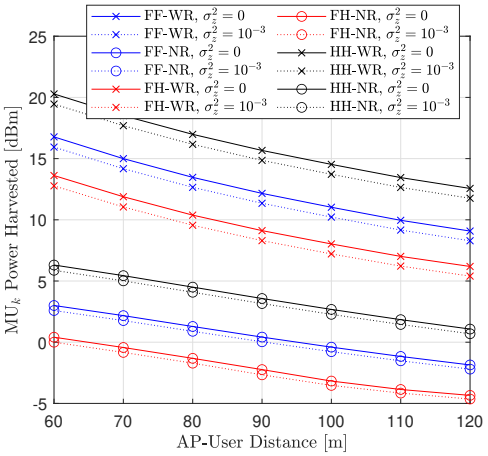

(b) MU_k harvested power vs AP-User distance [m].

Fig. 9: Effects of AP-User distance on system performance.

the FF-WR system shows a better performance (about 1.9 bps/s/Hz, at $\sigma^2_{\hat{G}_i} = -70$ dBm) than the FH-WR system. This performance gain can be attributed to the negative influence of the MU grouping becoming predominant, because the RSI power effect is doubled with the MU grouping. This is evident in the approximately similar gains difference observed before and after −90 dBm. The FD NR systems show similar behavior while outperforming HD NR at low RSI. Furthermore, across all RSI regimes, it is observed that the sum-rate remains unchanged in the HD systems. This is because the HD system is independent of SI. However, considering $(-110 > \sigma^2_{\hat{G}_i} > -80)$ dBm, both HH-WR and HH-NR systems outperform both FD systems because of the high RSI values present in the FD systems. Fig. 7b also shows the impact of the RSI power on the power harvested by each MU_k. It can be observed for all systems that the power harvested by each MU_k is unaffected by RSI during the EH stage. As the RSI power increases, the power harvested by each MU_k remains unchanged since the DL energy beamformer is unaffected by SI and can only affect the UL decoder.

Fig. 8 shows the impact of RIS elements on the system performance. The FH-WR system show significant sum-rate gain across the increased N elements. With $N = 60$, the sum-rate gain of FH-WR over FF-WR is approximately 2 bps/s/Hz. This is due to the lesser interference signal present in the FH-WR compared to the FF-WR. The NR systems have a constant sum-rate and MU amount of power harvested because no RIS is present. However, it can be observed that the FD NR systems outperform the HH-WR system when $N < 50$, and for $N > 50$, the HH-WR shows better performance over the FD-NR systems. This observation shows that setting the appropriate number of RIS elements is important to highlight the performance of an HD-WR system over FD NR systems. A similar observation can be seen in Fig. 8b. The amount of power harvested by each MU_k first increases and begins to saturate as the number of RIS elements increases ($N > 80$). This is because of the non-linearity (non-linear region) of the multi-stage rectifier EH circuit, hence, scaling the number of RIS elements only adds a small harvested power.

The illustration of the influence of varying the AP-MU distance on the sum-rate and power harvested in presented in Fig. 9. From Fig. 9a, it can be observed that increasing the distance of MU_k from the AP results in sharp sum-rate reduction. This is because as the distance increases, the MUs move further away from the AP and RIS. Meaning a reduction in the received signal strength due to signal attenuation. This increasing distance amplifies pathloss on both the direct AP-MUs links and the AP-RIS-MUs cascaded

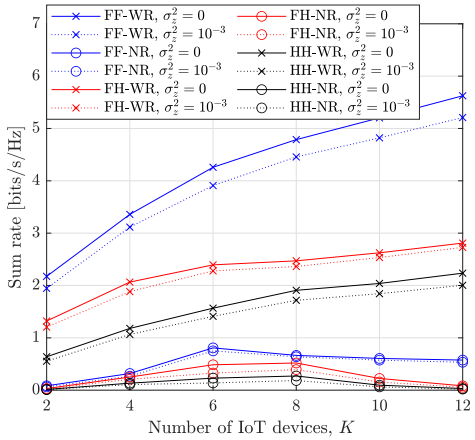

(a) Sum-rate vs number of IoT devices, K.

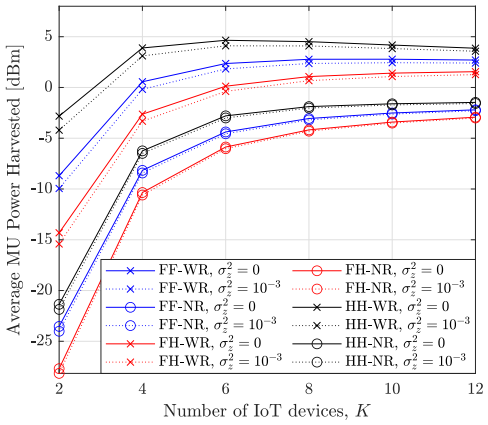

(b) MU_k harvested power vs number of IoT devices, K.

Fig. 10: Effects of number of MU_k on system performance.

links. Hence, the AP receives weaker signals during UL WIT, and the SINR drops. Again, as shown, under the considered system parameters ($P_{\max}^{\mathrm{UL}}$ = 20 dB and N = 60), the FH-WR scheme consistently outperforms the FF-WR scheme across all distances, reflecting its more favorable trade-off between interference management at certain instances and energy harvesting. Similarly, from Fig. 9b, the power harvested by MU_k decreases slowly when the distance between the AP and MUs increases. This is because the pathloss experienced on the links reduces the RF power incident on the rectifier network, hence, the signals received by the MU_k during WET are weaker.

Fig. 10 shows the effect of the increasing number of MUs on the system sum-rate performance. As illustrated in Fig. 10a, with a fixed $P_{\max}^{\mathrm{DL}}$ = 10 dB, it can be observed that the sum-rate initially improves sharply as the number of MUs, K, increases with few IoT devices (MU_k = 4), for all WR systems. This is because more power is harvested when the number of IoT devices increases between $2 > \mathrm{MU}_k < 6$, as shown in Fig.10b. However, the sum-rate attains saturation when the number of MUs increases beyond $\mathrm{MU}_k > 6$. This is due to the increased MU_k UL WIT interference from other MUs, coupled with the RSI. For all the NR systems, the system sum-rate first increases slightly due to the increase in power harvested as MUs increase (up to K = 6 MUs). However, for $\mathrm{MU}_k > 6$, the sum-rate reduces due to the absence of RIS beamforming gain with increased UL WIT interference from other MUs, and RSI. In Fig.10b, the average MU power harvested increases up to MU_k = 4, for both WR and NR systems. For the WR cases, when $\mathrm{MU}_k > 4$, the average MU power harvested starts to decrease due to the fixed power budget spread across more IoT devices, and the necessity of SI suppression, which affects the DL energy beamformer, hence affecting the power harvested. In the NR system, this is slightly different as the power harvested tends to saturate since the DL beamformer experiences reduced RSI due to the absence of the RIS.

VI. Conclusion

This paper has evaluated the spectral SE performance of an FD-FD RIS-assisted WPCN IIoT network using a practical EH model in which FD IIoT devices communicate with an FD-AP. The FD-AP and IIoT devices are equipped with dual-set multiple and dual-set single antennas, respectively, and both nodes operate in FD mode. First, an advanced multistage rectifier circuit EH model and rate expressions were derived for the proposed FD-FD system. For benchmarks, the derivations for an FD-HD system and an HD-HD system were presented. Using the WMMSE approach, iterative algorithms are developed to optimize the RIS phase shift, transmit, and receive beamformers in all schemes, while optimizing UE groupings and slot durations in the benchmark schemes for UL sumrate maximization. The simulation results showed the superiority of the proposed system model over benchmarks in special instances. Other issues that can be addressed in the future are multi-user scheduling effects, circuit-level validation of loop-back SI recycling efficiency, and energy efficiency analysis.

Appendix A
Multi-Stage Rectifier EH Model Derivation

As shown Fig. 2, an expression for the energy harvested at each MU_k is derived. The EH expression is first derived for a simple single-stage rectifier (i.e., β_k=1) and the result derived is extended to β_k-stage scenario. Using [29], [30], [35]–[37], the derivations are shown. From the Shockley diode equation, the instantaneous current through the diode is defined as

$$i_{dio,k}(t) = i_{s,k}\left(\exp\left(\frac{V_{in,k}(t) - \hat{V}_{out,k}(t)}{\eta_k V_{\mathrm{T},k}}\right) - 1\right), \tag{48}$$

where, $V_{in,k}(t)$ is the input voltage of the EH circuit, $\hat{V}_{out}(t)$ is the voltage across the diode, $i_{s,k}$ is the saturation current, η_k is the ideality factor, and $V_{\mathrm{T},k}$ is the thermal voltage of the diode. For direct current (DC) analysis, a low-pass filter (LPF) is applied to remove the alternating current (AC) component. Hence, the DC component, $i_{dio,k}^{\mathrm{DC}}$ of the diode current of MU_k is approximated as

$$i_{dio,k}^{\mathrm{DC}} \approx i_{s,k}\exp\left(\frac{-\hat{V}_{out,k}}{\eta_k V_{\mathrm{T},k}}\right)\exp\left(\frac{f_{LPF}(V_{in,k}(t))}{\eta_k V_{\mathrm{T},k}}\right) - i_{s,k}, \tag{49}$$

Assume the DC current of MU_k, $i_{dio,k}^{\mathrm{DC}} \approx 0$ due to low received signal power and high impedance of $R_{\mathrm{ld},k}$. By applying the

Taylor series expansion up to the 4th order and neglecting the odd powers in $V_{in,k}$ because they do not contribute to the DC output, $\hat{V}_{out}$ of the single-stage rectifier becomes

$$\hat{V}_{out,k} = \eta_k V_{\mathrm{T},k} \ln\left[1 + \frac{f_{LPF}(V_{in,k}^2(t))}{2\eta_k^2 V_{\mathrm{T},k}^2} + \frac{f_{LPF}(V_{in,k}^4(t))}{24\eta_k^4 V_{\mathrm{T},k}^4}\right]. \tag{50}$$

By applying the approximation $\ln(1+x) \approx x$, for small x, the equation in (50) is expanded, hence the output voltage is written as

$$\hat{V}_{out,k} = \left(\frac{f_{LPF}(V_{in,k}^2(t))}{2\eta_k V_{\mathrm{T},k}} + \frac{f_{LPF}(V_{in,k}^4(t))}{24\eta_k^3 V_{\mathrm{T},k}^3}\right) \tag{51}$$

For the multi-stage rectifier ($\beta_k > 1$), the output voltage becomes $V_{out,k} = 2\beta_k \hat{V}_{out,k}$, hence deduced as

$$V_{out,k} = 2\beta_k \left[\frac{f_{LPF}(V_{in,k}^2(t))}{2\eta_k V_{\mathrm{T},k}} + \frac{f_{LPF}(V_{in,k}^3(t))}{24\eta_k^3 V_{\mathrm{T},k}^3}\right] \tag{52}$$

From the multi-stage rectifier voltage expression, the output voltage is derived as

$$V_{out,k} = \left(\frac{\beta_k f_{LPF}(V_{in,k}^2(t))}{\eta_k V_{\mathrm{T},k}} + \frac{\beta_k f_{LPF}(V_{in,k}^4(t))}{12\eta_k^3 V_{\mathrm{T},k}^3}\right) \tag{53}$$

Given that $V_{in,k}(t) = y_k^{\mathrm{ET}}(t)\sqrt{R_{\mathrm{At},k}}$ where $y_k^{\mathrm{ET}}(t) \triangleq y_k^{\mathrm{DL}}$, and $V_{in,k}(t)$ increases with $R_{\mathrm{At},k}$ as $V_{in,k}^2(t) = y_k^{\mathrm{ET}}(t)^2 R_{\mathrm{At},k}$, then the stored output power is defined as $\tilde{P}_k = V_{out,k}^2/R_{\mathrm{ld},k}$, where $R_{\mathrm{ld},k}$ denotes the system power load of MU_k. Hence, we can write the expression

$$V_{out,k} = \left(\frac{\beta_k R_{\mathrm{At},k} f_{LPF}(y_k^{\mathrm{ET}}(t)^2)}{\eta_k V_{\mathrm{T},k}} + \frac{\beta_k R_{\mathrm{At},k}^2 f_{LPF}(y_k^{\mathrm{ET}}(t)^4)}{12\eta_k^3 V_{\mathrm{T},k}^3}\right) \tag{54}$$

Finally, the β_k-stage DC output voltage is derived as

$$V_{out,k} \approx \sum_{k=1}^{K}\left(\sum_{u\ \mathrm{even}, u\geq 2}^{U} \nu_{u,k}\alpha_{u,k} q_k^{\mathrm{ET}^{u/2}}\right), \tag{55}$$

where $q_k^{\mathrm{ET}} = \sum_{k=1}^{K} |\mathbf{h}_{\mathrm{e},k}\mathbf{p}_k|^2 + |\sqrt{P_k^{\mathrm{UL}}}\mathbf{h}_{\mathrm{ER},k}|^2$, $\nu_{2,k} = \beta_k R_{\mathrm{At},k}/\eta_k V_{\mathrm{T},k}$, $\nu_{4,k} = \beta_k R_{\mathrm{At},k}^2/12\eta_k^3 V_{\mathrm{T},k}^3$, $U = 4$, $\alpha_{2,k} = 1/2$, and $\alpha_{4,k} = 3/8$. By squaring (55), the derived expression for the output DC voltage can be simplified as

$$V_{out,k}^2 = \left(\frac{\alpha_{2,k}\beta_k R_{\mathrm{At},k}(\sum_{k=1}^{K} |\mathbf{h}_{\mathrm{e},k}\mathbf{p}_k|^2 + P_k^{\mathrm{UL}}|\mathbf{h}_{\mathrm{ER},k}|^2)}{\eta_k V_{\mathrm{T},k}} + \frac{\alpha_{4,k}\beta_k R_{\mathrm{At},k}^2(\sum_{k=1}^{K} |\mathbf{h}_{\mathrm{e},k}\mathbf{p}_k|^2 + P_k^{\mathrm{UL}^2}|\mathbf{h}_{\mathrm{ER},k}|^2)^2}{\eta_k^3 V_{\mathrm{T},k}^3}\right)^2 \tag{56}$$

The harvested output power for the FD-FD system is defined as $\tilde{P}_k^{\mathrm{EH}} = \frac{V_{out,k}^2}{R_{\mathrm{ld},k}}$, with its expanded version presented in 3 of Section III. Similarly, the derivation for the FD-HD and HD-HD follow the steps presented for the FD-FD. Hence, the FD-HD and HD-HD harvested output power is deduced as $\tilde{P}_{k,l}^{\mathrm{EH}} = \frac{\tau_l V_{out,k}^2}{\tau_j R_{\mathrm{ld},k}}$ with the expanded equation presented in (10). ■

—

References

[1] R. Akwafo, S. Menanor, D. K. P. Asiedu, S. Saoudi, and K.-J. Lee, "Multi-user Full-Duplex reconfigurable intelligent surface-assisted wireless powered IIoT networks," in *Proc. IEEE Veh. Technol. Conf. - Spring*, Jun. 2025, pp. 1–6.

[2] Y. Ren, R. Xie, F. R. Yu, T. Huang, and Y. Liu, "Potential identity resolution systems for the industrial internet of things: A survey," *IEEE Commun. Surveys Tut.*, vol. 23, no. 1, pp. 391–430, Dec. 2020.

[3] M. Alabadi, A. Habbal, and X. Wei, "Industrial internet of things: Requirements, architecture, challenges, and future research directions," *IEEE Access*, vol. 10, pp. 66 374–66 400, May 2022.

[4] C. Paniagua and J. Delsing, "Industrial frameworks for internet of things: A survey," *IEEE Sys. J.*, vol. 15, no. 1, pp. 1149–1159, May 2020.

[5] C. Peng and Y. Zhang, "Industrial Internet of Things intrusion detection model integrating graph attention network and gated temporal convolutional network," in *Proc. Int. Conf. Adv. Algorithms and Control Eng.* IEEE, Jun. 2024, pp. 596–599.

[6] B. Babayigit and M. Abubaker, "Industrial Internet of Things: A review of improvements over traditional scada systems for industrial automation," *IEEE Sys. J.*, vol. 18, no. 1, pp. 120–133, May 2023.

[7] B. Lyu, P. Ramezani, D. T. Hoang, S. Gong, Z. Yang, and A. Jamalipour, "Optimized energy and information relaying in self-sustainable IRS-empowered WPCN," *IEEE Trans. Commun.*, vol. 69, no. 1, pp. 619–633, Oct. 2020.

[8] D. K. P. Asiedu, S. Mahama, C. Song, D. Kim, and K.-J. Lee, "Beamforming and resource allocation for multiuser full-duplex wireless-powered communications in IoT networks," *IEEE Internet of Things J.*, vol. 7, no. 12, pp. 11 355–11 370, May 2020.

[9] J. Zhang, J. Tang, W. Feng, X. Y. Zhang, D. K. C. So, K.-K. Wong, and J. A. Chambers, "Throughput maximization for RIS-assisted UAV-enabled WPCN," *IEEE Access*, vol. 12, pp. 13 418–13 430, Jan. 2024.

[10] Z. Liu, X. Song, Y. Zhao, W. Zhao, and H. Wu, "RIS-aided Full-Duplex wireless powered communication network: Dynamic beamforming or static beamforming?" in *Proc. Int. Conf. Electronic Eng. Informatics (EEI)*. IEEE, Oct. 2024, pp. 1606–1610.

[11] S. Shin, P. Anokye, H. Lee, J. Moon, and K.-J. Lee, "Balancing available energy distribution in mMIMO SWIPT sensor networks with low resolution ADC/DAC," *IEEE Access*, vol. 12, pp. 128 702–128 716, Sep. 2024.

[12] Z. Chu, P. Xiao, D. Mi, W. Hao, M. Khalily, and L.-L. Yang, "A novel transmission policy for intelligent reflecting surface assisted wireless powered sensor networks," *IEEE J. Sel. Topics Signal Process.*, vol. 15, no. 5, pp. 1143–1158, Aug. 2021.

[13] S. Chen, F. Qin, B. Hu, X. Li, and Z. Chen, "User-centric ultra-dense networks for 5G: Challenges, methodologies, and directions," *IEEE Wireless Commun.*, vol. 23, no. 2, pp. 78–85, May 2016.

[14] M. Di Renzo, A. Zappone, M. Debbah, M.-S. Alouini, C. Yuen, J. De Rosny, and S. Tretyakov, "Smart radio environments empowered by reconfigurable intelligent surfaces: How it works, state of research, and the road ahead," *IEEE J. Sel. Areas Commun.*, vol. 38, no. 11, pp. 2450–2525, Nov. 2020.

[15] C. Qiu, Q. Wu, M. Hua, W. Chen, S. Ma, F. Hou, D. W. K. Ng, and A. L. Swindlehurst, "Intelligent reflecting surface empowered self-interference cancellation in full-duplex systems," *IEEE Trans. Commun.*, vol. 72, pp. 2945 – 2958, May 2024.

[16] Z. Zhu, Z. Li, Z. Chu, Q. Wu, J. Liang, Y. Xiao, P. Liu, and I. Lee, "Intelligent reflecting surface-assisted wireless powered heterogeneous networks," *IEEE Trans. Wireless Commun.*, vol. 22, no. 12, pp. 9881–9892, May 2023.

[17] Z. Zhu, Z. Li, Z. Chu, G. Sun, W. Hao, P. Liu, and I. Lee, "Resource allocation for intelligent reflecting surface assisted wireless powered IoT systems with power splitting," *IEEE Trans. Wireless Commun.*, vol. 21, no. 5, pp. 2987–2998, May 2021.

[18] S. Tewes, M. Heinrichs, P. Staat, R. Kronberger, and A. Sezgin, "Full-duplex meets reconfigurable surfaces: RIS-assisted SIC for full-duplex radios," in *ICC 2022-IEEE Int. Conf. on Commun.* IEEE, Aug. 2022, pp. 1106–1111.

[19] J. Hu, Y. Zheng, and K. Yang, "Multi-domain resource scheduling for full-duplex aided wireless powered communication network," *IEEE Trans. on Vehicular Technology*, vol. 71, no. 10, pp. 10 849–10 862, Oct. 2022.

[20] L. Cantos and Y. H. Kim, "IRS assisted wireless powered communication: Active or passive?" in *Proc. IEEE Int. Conf. Info. Commun. Technol. Convergence*, Oct. 2022, pp. 184–186.

[21] W. Zhang, Z. Wen, C. Du, Y. Jiang, and B. Zhou, "RIS-assisted self-interference mitigation for in-band full-duplex transceivers," *IEEE Trans. Commun.*, vol. 71, no. 9, pp. 5444–5454, Sep. 2023.

[22] T. Ji, M. Hua, C. Li, Y. Huang, and L. Yang, "Exploiting intelligent reflecting surface for enhancing full-duplex wireless-powered communication networks," *IEEE Trans. on Commun.*, vol. 72, pp. 553–569, Oct. 2023.

[23] M. Hua and Q. Wu, "Throughput maximization for IRS-aided MIMO FD-WPCN with non-linear EH model," *IEEE Journal of Selected Topics in Signal Process.*, vol. 16, no. 5, pp. 918–932, Aug. 2022.

[24] H. Ju and R. Zhang, "Throughput maximization in wireless powered communication networks," *IEEE Trans. Wireless Commun.*, vol. 13, no. 1, pp. 418–428, Dec. 2013.

[25] H. Chen, Y. Li, J. L. Rebelatto, B. F. Uchoa-Filho, and B. Vucetic, "Harvest-then-cooperate: Wireless-powered cooperative communications," *IEEE Trans. Signal Process.*, vol. 63, no. 7, pp. 1700–1711, Apr. 2015.

[26] X. Di, K. Xiong, P. Fan, H.-C. Yang, and K. B. Letaief, "Optimal resource allocation in wireless powered communication networks with user cooperation," *IEEE Trans. Wireless Commun.*, vol. 16, no. 12, pp. 7936–7949, Sep. 2017.

[27] Y. Zeng, H. Chen, and R. Zhang, "Bidirectional wireless information and power transfer with a helping relay," *IEEE Commun. Lett.*, vol. 20, no. 5, pp. 862–865, May 2016.

[28] C. Zhong, H. A. Suraweera, G. Zheng, I. Krikidis, and Z. Zhang, "Wireless information and power transfer with full duplex relaying," *IEEE Trans. Commun.*, vol. 62, no. 10, pp. 3447–3461, Oct. 2014.

[29] D. K. P. Asiedu and J.-H. Yun, "Full-duplex multiuser wireless information and power transfer with a multistage nonlinear rectifier energy harvesting model," *IEEE Wireless Commun. Lett.*, vol. 13, no. 1, pp. 183–187, Oct. 2023.

[30] D. Asiedu, S. Menanor, M. Benjillali, K. J. Lee, J.-H. Yun, and S. Saoudi, "An energy-efficient MU-MIMO and IRS backcom symbiotic radio network resource allocation," in *Proc. IEEE Wireless Commun. Networking Conf.* IEEE, Jul. 2024, pp. 1–6.

[31] C. Hu, L. Dai, S. Han, and X. Wang, "Two-timescale channel estimation for reconfigurable intelligent surface aided wireless communications," *IEEE Trans. Commun.*, vol. 69, no. 11, pp. 7736–7747, Apr. 2021.

[32] Z. Peng, Z. Zhang, C. Pan, L. Li, and A. L. Swindlehurst, "Multiuser full-duplex two-way communications via intelligent reflecting surface," *IEEE Trans. Signal Process.*, vol. 69, pp. 837–851, Jan. 2021.

[33] J. Dai, Y. Wang, C. Pan, K. Zhi, H. Ren, and K. Wang, "Reconfigurable intelligent surface aided massive MIMO systems with low-resolution DACs," *IEEE Commun. Lett.*, vol. 25, no. 9, pp. 3124–3128, Jul. 2021.

[34] D. K. P. Asiedu, K. E. Bennin, M. Benjillali, and S. Saoudi, "Energy efficient device-to-device routing in three-tier symbiotic radio IoT networks," in *Proc. IEEE Wireless Commun. Network. Conf.* IEEE, Mar. 2025, pp. 1–6.

[35] B. Clerckx and E. Bayguzina, "Waveform design for wireless power transfer," *IEEE Trans. Signal Process.*, vol. 64, no. 23, pp. 6313–6328, Dec 2016.

[36] B. Clerckx, R. Zhang, R. Schober, D. W. K. Ng, D. I. Kim, and H. V. Poor, "Fundamentals of wireless information and power transfer: From RF energy harvester models to signal and system designs," *IEEE J. Sel. Areas Commun.*, vol. 37, no. 1, pp. 4–33, Sep. 2018.

[37] S. García-Moreno, M. A. Gurrola-Navarro, C. A. Bonilla-Barragán, and I. Mejía, "Design method for RF energy harvesting rectifiers," *IEEE Trans. Circuits Systems II: Express Briefs*, vol. 67, no. 11, pp. 2727–2731, Jan. 2020.

[38] D. H. Nguyen, L. B. Le, and Z. Han, "Optimal uplink and downlink channel assignment in a full-duplex multiuser system," in *2016 IEEE Int. Conf. Commun.* IEEE, May 2016, pp. 1–6.

[39] F. Liu, X. Dai, M. Jin, W. Zhang, Y. Yang, and F. Qin, "TACAN: The shaping of delay distribution under multipath fading channel for industrial IoT systems," *IEEE Internet of Things J.*, vol. 9, no. 17, pp. 16 714–16 725, Sept. 2022.